# On the Ocean's Large-Scale Circulation near the Limit of No Vertical Mixing

J. R. TOGGWEILER AND B. SAMUELS

*Geophysical Fluid Dynamics Laboratory/NOAA, Princeton, New Jersey*

(Manuscript received 25 October 1996, in final form 10 December 1997)

ABSTRACT

By convention, the ocean's large-scale circulation is assumed to be a thermohaline overturning driven by the addition and extraction of buoyancy at the surface and vertical mixing in the interior. Previous work suggests that the overturning should die out as vertical mixing rates are reduced to zero. In this paper, a formal energy analysis is applied to a series of ocean general circulation models to evaluate changes in the large-scale circulation over a range of vertical mixing rates. Two different model configurations are used. One has an open zonal channel and an Antarctic Circumpolar Current (ACC). The other configuration does not. The authors find that a vigorous large-scale circulation persists at the limit of no mixing in the model with a wind-driven ACC. A wind-powered overturning circulation linked to the ACC can exist without vertical mixing and without much energy input from surface buoyancy forces.

## 1. Introduction

Equator-to-pole differences in the density of seawater allow cold high-latitude surface waters to sink below warmer waters in low latitudes. Sinking in high latitudes sets up a large-scale meridional circulation in which warm water flows poleward and is cooled to densities that permit sinking. According to radiocarbon evidence, sinking water replaces all the deep water in the ocean every 1000 years or so, requiring a total overturning rate of 20–40 Sv ($\text{Sv} \equiv 10^6\ \text{m}^3\ \text{s}^{-1}$: Stuiver et al. 1983; Broecker 1991). High-latitude surface waters also become dense in areas where evaporation and/or brine rejection increase the salt content of the sinking water. The combination of heat and salt effects gives rise to the notion that the ocean's large-scale meridional flow is mainly a ''thermohaline circulation'' driven by the addition or extraction of buoyancy at the ocean's surface.

In his essay on the deep circulation of the World Ocean, Warrren (1981) points out that surface heating and cooling are not enough to explain the existence of a thermohaline circulation. Warren argues that the net transfer of heat between the ocean and atmosphere is really a passive response to a circulation that is forced some other way. Oceanographers have supposed for many years that small-scale turbulent motions in the ocean's interior might be the main driving force for the thermohaline circulation. Turbulent mixing in the interior is thought to gradually warm the interior so that dense bottom waters from the poles can slowly displace old deep water upward in a broad diffuse upwelling.

This kind of circulation is readily demonstrated in general circulation models (GCMs). Using a model of an idealized sector ocean, F. Bryan (1987) showed that larger vertical mixing rates increase interior density differences and produce more overturning and a stronger poleward heat transport. In validation of Warren's argument, Bryan found that surface heat and salt fluxes are very small when there is no vertical mixing to support the overturning. As expected from earlier work (e.g. Munk 1966), vertical mixing rates of at least 1 $\text{cm}^2\ \text{s}^{-1}$ are needed to maintain the overturning and heat transport at levels close to their estimated values.

Direct attempts to measure the mixing effect in the ocean have generally found an order of magnitude less mixing than is called for in Bryan's model (Ledwell et al. 1993; Toole et al. 1994). Oceanographers continue to look for the missing mixing in the form of enhanced mixing near boundaries or rough topography (Polzin et al. 1997), but the prospect of finding enough mixing to sustain ~20 Sv of thermohaline overturning does not seem very good. Toggweiler and Samuels (1993) suggested that the removal of old deep water from the ocean's interior does not occur as a broad diffuse upwelling, but as a wind-forced upwelling south of the Antarctic Circumpolar Current (ACC). A GCM experiment carried out in Toggweiler and Samuels (1995) showed that the production of North Atlantic Deep Water scales with the wind forcing of the ACC and the upwelling rate south of the current. Vertical mixing might not be so critical if the large-scale overturning is linked to the ACC.

*Corresponding author address:* Dr. J. R. Toggweiler, GFDL/NOAA, P.O. Box 308, Princeton, NJ 08542.
E-mail: jrt@gfdl.gov

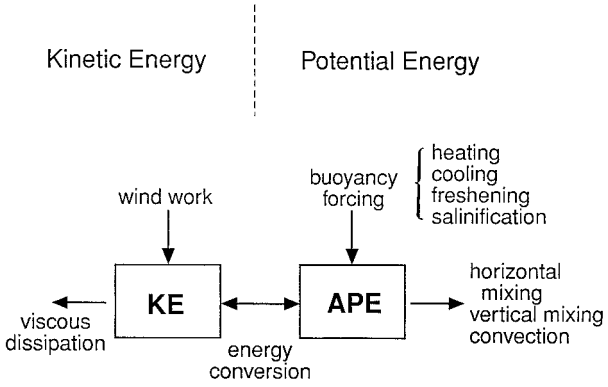


FIG. 1. Schematic of the ocean's mechanical energy budget. Individual source and sink terms are identified.

In this paper, the relative roles of vertical mixing and the ACC are examined through a formal analysis of the ocean's mechanical energy budget. The first part of the paper describes the energy analysis. Output from two GCMs is compared. One is the global model used by Toggweiler and Samuels (1993, 1995), which includes an open circumpolar channel and an ACC. The other is the idealized sector model of F. Bryan (1987), which does not have a circumpolar channel. In the second part of the paper, vertical mixing rates are varied systematically in the two models. Model results and energy diagnostics are extrapolated to zero mixing to reveal characteristics of the large-scale circulation near this limit.

## 2. The ocean's mechanical energy budget

The ocean's mechanical energy budget is illustrated in Fig. 1. As in other mechanical systems, the budget is divided into kinetic energy (KE) and potential energy (PE) components. Total kinetic energy in the ocean is derived simply by evaluating $mv^2/2$ for every parcel of fluid. This is hard to do for the real ocean, but it is trivial in a GCM where the velocity field is known at every point. Sources and sinks of kinetic energy are indicated by the arrows pointing downward and out to the left of the KE box. The work done by the wind to generate KE and the work done by viscous forces to dissipate KE are easily evaluated in models (Holland 1975).

The relevant form of potential energy in a stratified fluid like the ocean is the energy stored in horizontal variations of the density field. This quantity is known as available potential energy (APE). Sources and sinks of APE in Fig. 1 are indicated by the labels attached to the arrows. The arrow pointing downward into the APE box represents the work done by buoyancy forces to generate density anomalies. The arrow pointing outward to the right represents the work done by mixing and convection to dissipate these anomalies. Sources and sinks of APE are not easy to evaluate in ocean models. We are pleased to find that the arrows going into and out of the APE box can usually be balanced within ~10%.

The two-headed arrow between the KE and APE boxes represents the conversion of KE into APE and vice versa. The sign and magnitude of the energy conversion term is a pointer as to which kind of forcing, wind or buoyancy, is dominating the production of APE. If buoyancy forces dominate, mechanical energy is released from the density field in the form of meridional boundary currents that dissipate energy frictionally. As with the sources and sinks of kinetic energy, the energy conversion term is easily evaluated in ocean models.

### *a. APE as illustrated by the "flattening bowl"*

Imagine an ocean composed of two volumes of water, one lower in density than the other. Assume that the two volumes are arranged so that a bowl-shaped volume of the low-density water floats in the denser volume, much as the warm water above the thermocline resides in the real ocean. Assume that there is no mixing between the volumes and that some unspecified set of forces maintains the two volumes in this configuration. Now imagine that the forcing can be turned off so that the density field is allowed to relax.

During the relaxation, water parcels in the low-density fluid spread outward near the surface while the bottom level of the low-density fluid rises, that is, the bowl becomes flatter and thinner. Eventually all the low-density water will rest over the dense water in a flat sheet of uniform thickness. The final state has no available potential energy: all the APE in the initial density distribution has been converted into KE during the relaxation. The APE of the initial state is simply the difference in potential energy between the initial and final states as in (1):

$$\text{APE} = \int \rho_i g h_i \, dV - \int \rho_f g h_f \, dV, \qquad (1)$$

where $\rho$ is the local density, either low or high; $g$ is the acceleration due to gravity; and $h$ is the height above the bottom. The PE of the initial state is greater than the potential energy of the final state because some of the high-density fluid in the initial state stands relatively high in the water column around the perimeter of the low-density bowl.

The conversion of potential energy into kinetic energy can be calculated by integrating the local covariance between density anomaly and vertical motion during the relaxation as in (2):

$$B = -g \int (\rho - \tilde{\rho}) w \, dV. \qquad (2)$$

Here $\rho$ is a local density and $\tilde{\rho}$ is the average density at a given $h$, and $w$ is the vertical velocity. By definition,

the energy conversion term $B$ applies to both PE and APE. Vertical motions in the flattening bowl convert PE into KE through the sinking of dense water around the perimeter of the bowl and the rising of light water in the center of the bowl. Both branches of this cycle produce a negative covariance between $\rho - \tilde{\rho}$ and $w$. By convention, $B$ is assumed to have a positive sign if PE is converted into KE, hence the negative sign in front of the integral in (2).

The energy conversion term represents work done to produce or release potential energy from the mean stratification. In the case of the flattening bowl, potential energy is released as the walls of the bowl become flatter and the average vertical stability increases. The center of mass at the end of the relaxation is lower as denser water sits closer to the center of the earth.

### b. The Lorenz approximation

Exact specification of APE in the ocean requires knowledge of a theoretical reference state in which all parcels of the fluid can be rearranged reversibly and adiabatically to a state of minimum potential energy (Oort et al. 1989). The reference state in the flattening bowl example is simply the final resting state of the system where two slabs of uniform density lie one over the other. Finding the reference state for the real ocean, where the density of seawater is a complicated function of temperature, salinity, and pressure, is considerably more difficult.

APE will be evaluated here by using the Lorenz approximation (Lorenz 1955), for which specification of the reference state is not needed. The Lorenz approximation is a linearized form of APE that was originally based on the determination of local potential temperature anomalies in the atmosphere with respect to the horizontal mean. It has been applied to the ocean in studies by Bryan and Lewis (1979) and Bryan (1987). Oort et al. (1989) mapped the APE distribution in the ocean's interior using the Lorenz approximation and the Levitus (1982) dataset for temperature and salinity.

APE is defined here in Eq. (3) following the notation of Oort et al. (1989):

$$\text{APE} = -\frac{1}{2}g \int \frac{(\rho - \tilde{\rho})^2}{\partial \tilde{\rho}_\theta/\partial z}\, dV. \tag{3}$$

In a system where density is described by a full equation of state, $\rho$ is a local in situ density and $\tilde{\rho}$ is the average in situ density at the local depth. Here $\partial \tilde{\rho}_\theta/\partial z$ is the vertical stability of the horizontally averaged density expressed in terms of the change in potential density with depth. A density anomaly of either sign contributes positively to APE since the anomaly term in (3) is squared.

Oort et al. (1994, hereafter OAP94) evaluated sources and sinks of oceanic APE by taking the time derivative of (3) under the assumption that $\tilde{\rho}$ and $\partial \tilde{\rho}_\theta/\partial z$ are relatively time invariant. The resulting expression for the derivative (4)

$$\frac{\partial \text{APE}}{\partial t} = -g \int \frac{(\rho - \tilde{\rho})\dot{\rho}}{\partial \tilde{\rho}_\theta/\partial z}\, dV \tag{4}$$

has one time-dependent variable, the term $\dot{\rho}$ which appears in the numerator. OAP94 used observation-based estimates of surface heat and water fluxes to evaluate $\dot{\rho}$ in (4) in order to compare the energetic effects of surface fluxes with other components of the energy budget. OAP94 could not evaluate the effects of advection or mixing from observational data.

Following the approach of OAP94, one can use (4) to evaluate APE sources and sinks in ocean models. The full model density tendency equation is given in (5):

$$\frac{\partial \rho}{\partial t} = -\mathbf{u}\cdot\boldsymbol{\nabla}_h\rho - w\frac{\partial \rho}{\partial z} + A_{hh}\nabla_h^2\rho + \frac{\partial}{\partial z}\left(A_{hv}\frac{\partial \rho}{\partial z}\right) + \gamma(\rho^* - \rho). \tag{5}$$

Here, $-\mathbf{u}\cdot\boldsymbol{\nabla}_h\rho$ is the change in density due to horizontal advection, $-w\partial\rho/\partial z$ is the change in density due to vertical advection, $A_{hh}\nabla_h^2\rho$ is the change in density due to horizontal mixing,

$$\frac{\partial}{\partial z}\left(A_{hv}\frac{\partial \rho}{\partial z}\right)$$

is the change in density due to vertical mixing, and $\gamma(\rho^* - \rho)$ is the surface forcing expressed as a restoring toward observed densities $\rho^*$ with an inverse time constant $\gamma$. The global APE balance takes the form of (6) where each term on the right-hand side of (5) is substituted into (4):

$$\frac{\partial \text{APE}}{\partial t} = g \int \frac{(\rho - \tilde{\rho})\mathbf{u}\cdot\boldsymbol{\nabla}_h\rho}{\dfrac{\partial \tilde{\rho}_\theta}{\partial z}}\, dV + g \int \frac{(\rho - \tilde{\rho})w\dfrac{\partial \rho}{\partial z}}{\dfrac{\partial \tilde{\rho}_\theta}{\partial z}}\, dV - g \int \frac{(\rho - \tilde{\rho})A_{hh}\nabla_h^2\rho}{\dfrac{\partial \tilde{\rho}_\theta}{\partial z}}\, dV \ldots \tag{6}$$

Individual density tendency terms in (5) are evaluated in a GCM by pulling out the corresponding terms for potential temperature and salinity. Temperature and salinity tendencies at each grid point are multiplied by the coefficients of thermal and haline expansion, $\partial\rho/\partial T$ and $\partial\rho/\partial S$, respectively, which are evaluated using the UNESCO equation of state (Gill 1982) at the in situ pressure. The temperature and salinity effects are then added together to produce the density tendencies in (5), which are substituted into (6).

TABLE 1. Description of models.

| Model | $A_{hv}$ ($cm^2 s^{-1}$) | Description |
|---|---|---|
| | | Sector models |
| S0.1 | 0.1 | ''Bowl'' geometry version of sector model described in F. Bryan (1987). Version S1.0 is used for comparison with standard global model. |
| S0.5 | 0.5 | |
| S1.0 | 1.0 | |
| S2.5 | 2.5 | |
| Asymmetric | 1.0 | Sector model with asymmetric salinity field. Surface salt flux from S1.0 is used in place of salinity restoring. |
| | | Global models |
| Standard | 0.3–1.3 | Standard model in Toggweiler and Samuels (1995). Identical to the ''prognostic'' model of Toggweiler et al. (1989) except for minor changes noted in Toggweiler and Samuels (1993). |
| G0.1 | 0.1 | Depth-variable vertical mixing coefficients used in the standard global model are replaced with the constant coefficients used in S0.1, S0.5, S1.0, S2.5. |
| G0.5 | 0.5 | |
| G1.0 | 1.0 | |
| G2.5 | 2.5 | |
| Standard − no winds | 0.3–1.3 | Standard model with no wind stress applied anywhere. |
| N0.1 | 0.1 | Models G0.1, G0.5, G1.0 are re-run with no wind stress applied anywhere. |
| N0.5 | 0.5 | |
| N1.0 | 1.0 | |
| G30S | 0.3–1.3 | Standard model with wind stress applied only north of 30°S. |
| Nonsinking | 0.3–1.3 | Standard model in which an average of 2 salinity units is subtracted from salinities being restored to north of 35°N in the North Atlantic. |

The effects of surface fluxes can be determined directly from the changes in surface temperature and salinity produced by the model's restoring boundary conditions. Convective mixing in GCMs is generally carried out after model temperatures and salinities have been updated. The convective contribution to APE can be determined by evaluating the global change in APE using (3) before and after the convective mixing step is carried out. The stability term, $\partial\tilde{\rho}_\theta/\partial z$, is evaluated at the midpoint of each model layer using the local depth as the reference pressure for determining the potential density gradient. The stability factor for the model's surface layer is evaluated at the base of the surface layer rather than at the midpoint.

## 3. Comparison of energy budgets in two GCMs

The energy analysis in the previous section is applied next to two ocean models. One is a global model with realistic continents; the other describes an idealized sector of the ocean somewhat like the Atlantic Ocean (Bryan 1987). The global model being used in this study is the ''standard'' model of Toggweiler and Samuels (1993, 1995). Bryan's sector model is the prototype of many idealized studies of the thermohaline circulation. It is composed of two pie-shaped sectors 60° longitude wide joined together across the equator. The sector model has been modified here to include a ''bowl'' bathymetry (Winton 1997).

Both models have a grid resolution of 4.5° latitude by 3.75° longitude and 12 vertical levels. Grid spacing in the vertical is the same in both models. Both models are based on the GFDL MOM 1 code (Pacanowski et al. 1991). The numerical scheme used to represent the equations of motion in MOM was originally selected in order that the model's advective terms would be energy conserving (K. Bryan 1969).

The global model is forced by the annual mean wind stresses of Hellerman and Rosenstein (1983) and by restoring its surface temperatures and salinities ($\Delta z$ = 51 m) to an annual average of observations in the upper 50 m according to Levitus (1982). The time constants for restoring are 1/30 $day^{-1}$ for temperature and 1/120 $day^{-1}$ for salinity. The sector model is forced with a purely zonal wind stress field derived from the zonally and hemispherically averaged stresses used to drive the global model. The sector model's temperatures and salinities are forced by restoring to the zonally and hemispherically averaged quantities used to force the global model. Restoring constants in the sector model are 1/25 $day^{-1}$. No special mixed layer formulation is used in either model; the 51-m surface layer functions as both the mixed layer for temperature and salinity and the Ekman layer for momentum.

Both vertical and horizontal mixing coefficients for tracers vary with depth in the global model. The vertical mixing coefficient increases from 0.3 $cm^2\ s^{-1}$ in the upper kilometer to 1.3 $cm^2\ s^{-1}$ in the deepest kilometer, while the horizontal mixing coefficient decreases exponentially from $1.0 \times 10^7$ $cm^2\ s^{-1}$ at the surface to $0.5 \times 10^7$ $cm^2\ s^{-1}$ at the bottom (Bryan and Lewis 1979). Tracer mixing in the sector model is parameterized by constant coefficients, $1 \times 10^7$ $cm^2\ s^{-1}$ in the horizontal, and 1 $cm^2\ s^{-1}$ in the vertical. Lateral mixing of tracers is oriented strictly along horizontal surfaces in both models. The same coefficients for momentum mixing are employed in both models, $2.5 \times 10^9$ $cm^2\ s^{-1}$ in the horizontal and 20 $cm^2\ s^{-1}$ in the vertical. A

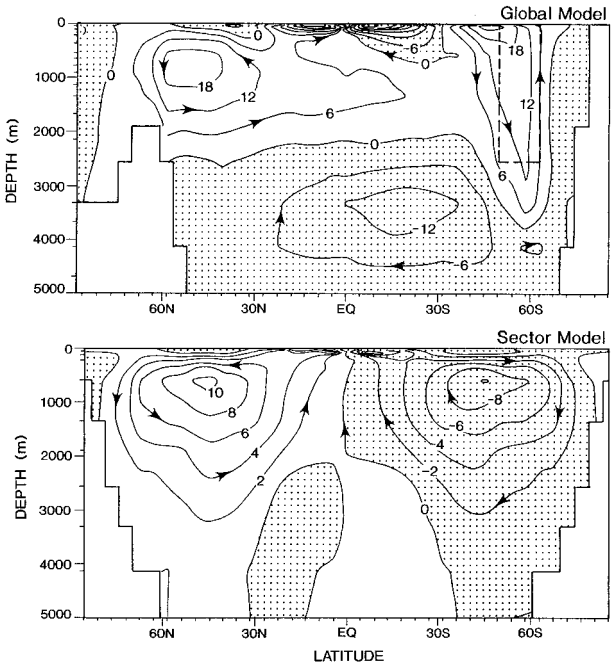


FIG. 2. Comparison of meridional overturning streamfunctions for the global model (top) and the sector model (bottom) described in the text. Flow between streamlines is 6 Sv in the global model and 2 Sv in the sector model. The dashed box centered on 60°S in the top panel shows the depth and latitudinal extent of the gap between South America and Antarctica in the global model.

larger set of global and sector models that have been run out with the same vertical mixing coefficients will be compared later. Additional information about the global and sector models is given in Table 1.

Figure 2 shows a comparison of the meridional overturning streamfunctions of the global and sector models. Overturning in the sector model consists of two symmetric cells in both hemispheres. About 6.5 Sv of new deep water sinks poleward of 60° in each hemisphere and flows equatorward below 1000 m. All of the sinking deep water upwells across 1000 m between 30°N and 30°S. About 26 Sv of new deep water sinks below 1000 m in the polar regions of the global model, but only 9 of the 26 Sv upwells across 1000 m between 30°N and 30°S. Fifteen Sverdrups of deep water upwells across 1000 m near 60°S in association with the Ekman divergence on the southern flank of the ACC. Overturning in the global model is much more vertically segregated with a strong southward flow between the hemispheres at middepth.

The contour intervals used to draw the streamfunction in Fig. 2 are 6 Sv for the global model and 2 Sv for the sector model. This distinction is made to reflect that the east–west extent of a typical zonal band in the global model is about three times wider than the 60° width of the sector model. Maximum poleward heat transport is $1.11 \times 10^{15}$ W at 20°N in the global model and $0.47 \times 10^{15}$ W at 36° in the sector model. Like the overturning, the heat transport in the two models is similar if normalized for longitudinal extent.

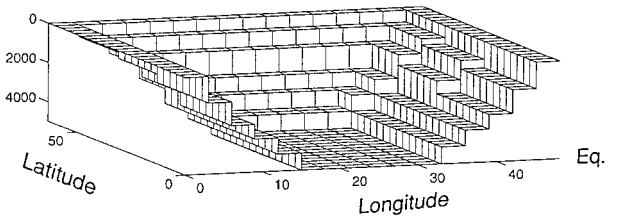


FIG. 3. Bowl geometry in a single hemisphere of the sector model as viewed from the equator. Graphic does not include the convergence of meridians toward the pole.

Figure 3 shows the bowl topography used in running the sector model. The original Bryan (1987) model has vertical walls along both its eastern and western boundaries. Winton (1997) has shown that a sector model with vertical walls produces an unrealistic downwelling where surface currents in the band of midlatitude westerlies strike the eastern boundary. Use of the bowl geometry in the sector model produces an overturning rate that is more consistent with the model's heat uptake and heat transport.

### *a. Sources and sinks of kinetic energy*

The time rate of change of kinetic energy can be determined by taking the scalar product of the local velocity vector with the individual terms in the horizontal momentum equation (7):

$$\frac{\partial \mathbf{u}}{\partial t} = -\mathbf{u}\cdot\nabla_h\mathbf{u} - w\frac{\partial \mathbf{u}}{\partial z} - f\mathbf{k}\times\mathbf{u} - \frac{1}{\rho_o}\nabla_h p + A_{mh}\nabla_h^2\mathbf{u} + A_{mv}\frac{\partial^2\mathbf{u}}{\partial z^2} + \mathrm{SF}. \quad (7)$$

Here $-\mathbf{u}\cdot\nabla_h\mathbf{u}$ and $-w\partial\mathbf{u}/\partial z$ are the horizontal and vertical advection of momentum, $-f\mathbf{k}\times\mathbf{u}$ is the Coriolis term, $-\rho_o^{-1}\nabla_h p$ is the pressure gradient term, $A_{mh}\nabla_h^2\mathbf{u}$ and $A_{mv}\partial^2\mathbf{u}/\partial z^2$ are momentum sinks due to the horizontal and vertical mixing of momentum respectively, and SF represents the surface forcing by the wind stress.

Most of the terms of the momentum equation have no effect on the production or dissipation of KE. The scalar product of the velocity vector and the Coriolis term is zero by definition. Holland (1975) has shown that sources and sinks of kinetic energy due to advection sum to zero over a closed volume. Similarly, the work done by advection operating on pressure gradients nearly vanishes when there is no flow at lateral and vertical boundaries. The work done by vertical motions to redistribute pressure differences internally remains as $-g\int \rho w\, dV$, the inter-conversion of APE and KE described in (2).

The global integral for KE is left with a limited number of terms with the form of (8):

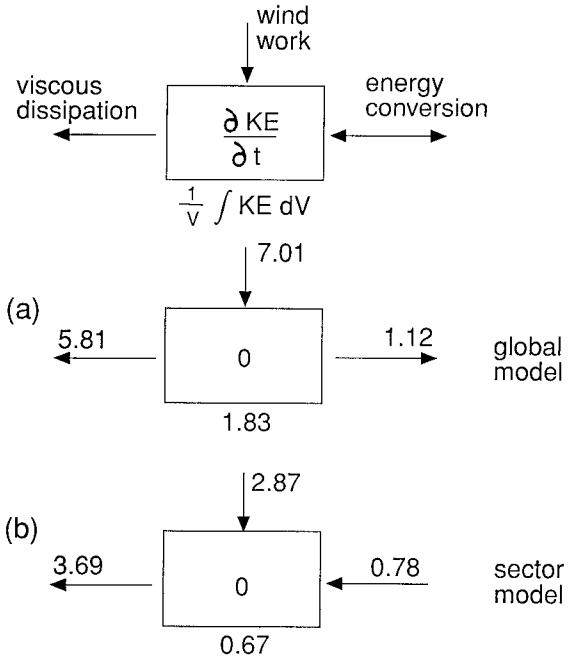


FIG. 4. Steady-state kinetic energy balance in the standard global model (a) and sector model S1.0 (b). Globally averaged sources and sinks are given next to the arrows (units $10^{-6}$ erg cm$^{-3}$/s). Average kinetic energy per unit volume is given below (erg cm$^{-3}$).

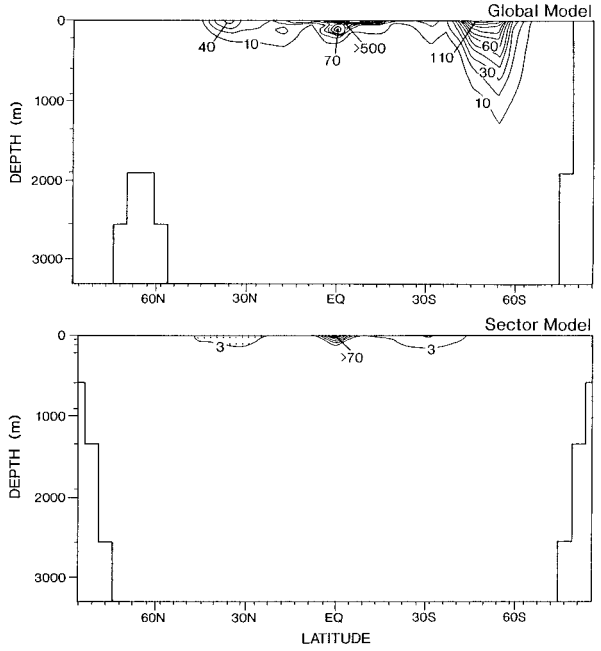


FIG. 5. Latitude versus depth distribution of zonally integrated kinetic energy in the standard global model (top) and sector model S1.0 (bottom) (units $10^9$ erg cm$^{-2}$).

$$\frac{\partial \mathrm{KE}}{\partial t} = W + B + D, \tag{8}$$

where $W$ represents the work done by the wind to generate KE, $B$ is the interconversion of APE and KE, and $D$ represents the dissipation of KE by viscous forces. Equation (8) has the same form as the box diagram in Fig. 1. Work done by the wind in driving the surface flow $W$ is evaluated by taking the scalar product of the local velocity vector in the model's first layer $\mathbf{u}_1$ with the wind stress vector $\tau$ and integrating over all surface grid points (9):

$$W = \int \mathbf{u}_1 \cdot \tau \, dA \tag{9}$$

Dissipation of kinetic energy, $D$, is evaluated by multiplying the local velocity vector with the frictional acceleration experienced by each parcel, as in (10).

$$D = \rho \int \mathbf{u}(A_{mh}\nabla_h^2 \mathbf{u} + A_{mv}\partial_{zz}\mathbf{u}) \, dV. \tag{10}$$

A separate drag coefficient is used to determine dissipation due to bottom friction.

The global kinetic energy balances derived from the fully spunup models are shown in Fig. 4. Results are given as an average energy density to eliminate the volume difference between the two models. The total kinetic energy density is 1.83 erg cm$^{-3}$ in the global model and 0.67 erg cm$^{-3}$ in the sector model. Work done by the wind in the global model is $7.01 \times 10^{-6}$ erg cm$^{-3}$/s. The comparable figure in the sector model is $2.63 \times 10^{-6}$ erg cm$^{-3}$/s. Thus, the global model has three times more KE per unit volume and the winds do nearly three times more work.

Kinetic energy is dissipated in the global model at a lower rate than it is put in by the winds, $-5.81 \times 10^{-6}$ versus $7.01 \times 10^{-6}$ erg cm$^{-3}$/s, reflecting a net KE $\rightarrow$ APE conversion of $1.12 \times 10^{-6}$ erg cm$^{-3}$/s. Kinetic energy is dissipated in the sector model at a greater rate than it is put in, $-3.69 \times 10^{-6}$ versus $2.87 \times 10^{-6}$ erg cm$^{-3}$/s, indicating a net conversion of $0.78 \times 10^{-6}$ erg cm$^{-3}$/s of APE to KE. All three terms in the kinetic energy balance, $W$, $B$, and $D$, are explicitly calculated. The time derivative is zero. As shown in Fig. 4, sources and sinks of kinetic energy balance in both the global and sector models within 1% or 2%.

Figure 5 compares the spatial distribution of kinetic energy for the global and sector models. Results are plotted as zonal integrals (units of $10^9$ erg cm$^{-2}$), which emphasize activities operating over the greatest distances that contribute most strongly to the global integral. As in Fig. 2, the contour interval is three times larger in the global model.

The ACC at 40°–60°S is the most important feature in the global model's kinetic energy field. Relatively high values of kinetic energy extend down to 1000 m. This result is not surprising in light of the fact that the upper 1000 m of the ACC consists of 5–10 cm s$^{-1}$ eastward flows around whole latitude circles. A very high value of kinetic energy also appears at the equator

TABLE 2. Individual terms in the energy balance ($10^{-6}$ ergs cm$^{-3}$/s).

| Model | KE balance | | Energy conversion | APE balance | | | |
|---|---|---|---|---|---|---|---|
| | $W$ | $D$ | $B$ | $H + V$ | $M$ | $K$ | $S$ |
| | | | Sector | | | | |
| S0.1 | 2.48 | −1.60 | −0.78 | 0.78 | −1.07 | −0.50 | 1.12 |
| S0.5 | 2.52 | −2.43 | −0.06 | 0.24 | −1.23 | −2.29 | 4.01 |
| **S1.0** | **2.87** | **−3.69** | **0.78** | **−0.26** | **−1.68** | **−4.42** | **7.46** |
| S2.5 | 2.93 | −7.05 | 3.81 | −1.80 | −2.78 | −9.9 | 17.0 |
| Asymmetric | 2.94 | −4.50 | 1.44 | −0.25 | −2.03 | −3.82 | 6.46 |
| | | | Global | | | | |
| G0.1 (Temperature and salinity fields compromised by extensive Peclet number violations) | | | | | | | |
| **Standard** | **7.01** | **−5.81** | **−1.12** | **1.32** | **−2.44** | **−1.10** | **2.18** |
| G0.5 | 7.32 | −6.45 | −0.81 | 0.87 | −2.61 | −1.59 | 3.30 |
| G1.0 | 7.89 | −7.79 | −0.09 | 0.35 | −3.46 | −3.04 | 5.97 |
| G2.5 | 8.57 | −13.0 | 4.0 | −1.95 | −5.0 | −7.8 | 14.3 |
| Standard − no winds | 0 | −0.86 | 0.74 | −0.15 | −0.88 | −1.07 | 2.01 |
| N0.1 | 0 | −0.21 | 0.18 | −0.07 | −0.35 | −0.38 | 0.79 |
| N0.5 | 0 | −1.32 | 1.15 | −0.49 | −1.09 | −1.67 | 3.14 |
| N1.0 | 0 | −2.83 | 2.48 | −1.02 | −1.93 | −3.24 | 5.94 |
| G30S | 3.12 | −3.40 | 0.14 | 0.78 | −1.62 | −1.20 | 2.27 |
| Nonsinking | 7.45 | −6.02 | −1.30 | 1.29 | −2.60 | −1.80 | 2.12 |

but is confined entirely to surface currents in the model's first layer. The sector model has large KE values only at the equator. Even though the wind stresses used in both models are essentially the same, the winds do nearly three times more work in the global model. This is possible because wind stresses applied in the latitude band of the ACC act on a current that moving at 10–15 cm s$^{-1}$ in the same direction as the applied stress. About 55% of the total kinetic energy generation in the global model occurs in the latitude band of the ACC. Some 50% of the KE generated in the ACC (or 25% of KE generation globally) is converted into APE (below).

### *b. Sources and sinks of APE in the global model*

The time rate of change of global APE in Eq. (6) can be represented symbolically as

$$\frac{\partial \text{APE}}{\partial t} = H + V + M + K + S, \qquad (11)$$

where $H$ and $V$ denote the sources and sinks of APE due to horizontal and vertical advection, $M$ denotes the dissipation of APE due to horizontal mixing, $K$ denotes the dissipation of APE due to vertical mixing, and $S$ denotes the sources of APE due to surface buoyancy forces. Table 2 lists all the source/sink terms for each model considered in this paper. Results from the standard global and sector models are highlighted with bold numbers.

In the absence of mixing and external forcing, advection is an adiabatic process and should not generate or dissipate APE. Thus, one expects advection to have relatively little effect on APE apart from the vertical component that is related to energy conversion $B$, Eq. (2). Evaluation of $H$ and $V$ in the global model yields two very large numbers of opposite sign, $63.84 \times 10^{-6}$ and $-62.50 \times 10^{-6}$ erg cm$^{-3}$/s, respectively. Their sum is $1.32 \times 10^{-6}$ erg cm$^{-3}$/s, a value similar to the net energy conversion evaluated in the global model, $-1.12 \times 10^{-6}$ erg cm$^{-3}$/s, but opposite in sign. Recall, however, that negative $B$, by convention, is a sink for KE and a source of APE. Thus, $H + V$ and $-B$ in the global model are nearly equal sources of APE. The results of $H + V$ for all the models considered in this paper are tabulated in Table 2, but we assume henceforth that $H + V$ can be replaced in the APE balance by $-B$. Any nonzero difference between $H + V$ and $-B$ is assumed to be an error in the APE approximation.

When the advective terms are replaced by $-B$, (11) reduces to (12) with the form of Fig. 1:

$$\frac{\partial \text{APE}}{\partial t} = S - B + (M + K). \qquad (12)$$

Figure 6 illustrates the global model's APE budget in the same form as Fig. 4. Again, each term is explicitly calculated, and the time derivative is zero.

Heating and cooling in the global model generates APE at a rate of $2.34 \times 10^{-6}$ erg cm$^{-3}$/s. Evaporation and precipitation produce a small negative contribution. The two effects added together provide a net APE source, $S$, of $2.18 \times 10^{-6}$ erg cm$^{-3}$/s. The total amount of work done by buoyancy forces is about one-third of the work done by the wind ($7.01 \times 10^{-6}$ units). The combined dissipation sink, $M + K$, is $3.54 \times 10^{-6}$ erg cm$^{-3}$/s. This is larger than the source $S$ because energy conversion $B$ adds $1.12 \times 10^{-6}$ erg cm$^{-3}$/s to the APE, which must also be dissipated. Horizontal mixing $M$ reduces model APE at a rate of $2.44 \times 10^{-6}$ erg cm$^{-3}$/s. The amount of APE dissipated by convection is negligible.

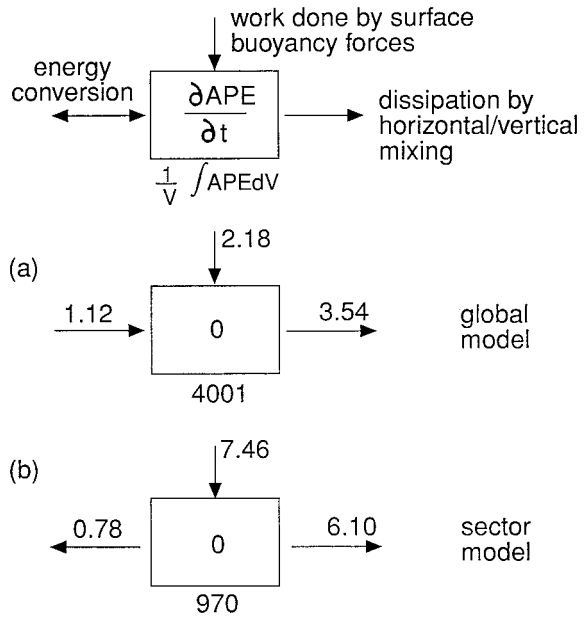


FIG. 6. Steady-state APE balance in the standard global model (a) and the sector model (b) ($10^{-6}$ erg cm$^{-3}$/s). Average APE per unit volume is given below erg cm$^{-3}$. The dissipative effects of horizontal and vertical mixing are combined.

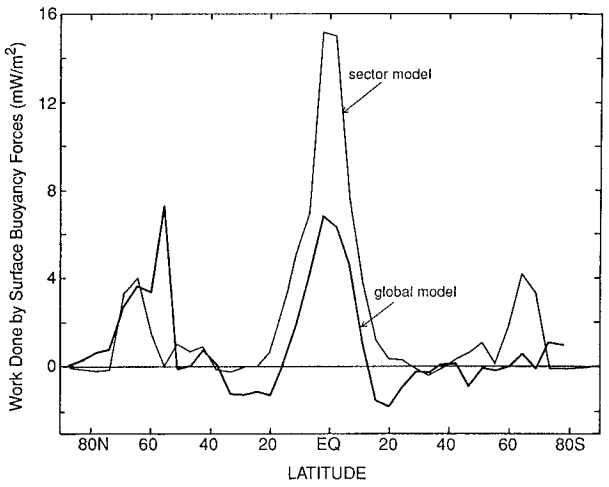


FIG. 7. Work done by surface buoyancy forces (heating/cooling plus freshening/salinification) in the standard global model and the sector model S1.0 plotted as a function of latitude. Results are simple zonal averages ($10^{-3}$ W m$^{-2}$).

Vertical mixing $K$ dissipates APE at a rate of $1.10 \times 10^{-6}$ erg cm$^{-3}$/s. Most of this effect is felt at the surface where vertical mixing cools the surface layer in the Tropics and negates the effect of surface heating. Although the direct effect of vertical mixing is to reduce APE, the total amount of work done by surface buoyancy forces is always about two times greater than the energy sink due to vertical mixing (Table 2). Thus, production of APE grows as vertical mixing increases, as one would expect. The production of APE by buoyancy forces, $S$, is twice the production of APE by energy conversion, $-B$, with the vertical mixing used in the standard global model.

The overall APE budget for the global model is out of balance by $-0.24 \times 10^{-6}$ ergs/cm$^3$/s, that is, the combined dissipation sink, $M + K$, exceeds APE sources, $S - B$. The imbalance is about 7% of the combined sources or the dissipation sink. The APE imbalance grows in absolute and relative terms as the vertical mixing is increased. This is because high levels of vertical mixing deform the density field and drive local densities farther from the horizontal mean. One expects the Lorenz approximation to produce larger errors with increased deformation.

Figure 7 shows the work done by surface buoyancy forces plotted as a function of latitude. Here the combined effects of heating/cooling and freshening/salinification are plotted as zonal averages in $10^{-3}$ W per m$^2$ of ocean surface, or mW m$^{-2}$. Surface buoyancy forces generate APE in the Tropics, where relatively light water is made lighter by surface heating. They also generate APE near 60°N in the North Atlantic where relatively dense water is made denser by surface cooling.[1] Most of the work done by heating and cooling in Fig. 7 scales one-for-one with the level of vertical mixing and the volume of deep water upwelled from below the thermocline.

Figure 7 shows that surface buoyancy forces release APE from the density field in the subtropics. This is a consequence of the shallow wind-driven overturning system (Fig. 2) in which water is upwelled and warmed up at the equator and then is cooled and pumped down again equatorward of 30°. Heating and cooling in this latitude band occurs in water with roughly the same density such that subtropical cooling partly negates the effect of tropical heating. The heating effect in the Tropics is greater than the cooling effect in the subtropics because of the cold water upwelled from below the thermocline. With no vertical mixing, no deep water upwells through the thermocline and the effect of tropical heat-

[1] The spike in Fig. 7 just south 60°N is a spurious feature that arises due to filtering. At latitudes greater than 45°N and 45°S the model's temperature and salinity fields are filtered to allow for a longer time step. Filtering in the grid row at 56°N tries to damp a sharp discontinuity in the salinity field between very fresh salinities in the Baltic Sea and higher salinities in the open ocean. The model's surface forcing, meanwhile, is based on the difference between observed salinities along 56°N, which are not filtered, and the model salinities, which are filtered. This distinction produces a spurious salt flux into the ocean in the first open ocean grid point seaward of the Baltic points (see Rahmstorf 1996 and reply by Toggweiler et al. 1996). The global model has been rerun with a shorter time step and the filtering latitude shifted to 60° from 45°. The circulation remains very similar while the spike is reduced to a few tenths of a milliwatt per square meter. The filter effect is exaggerated in Fig. 7 because the work done by surface buoyancy forces is given per unit area. The latitude belt at 56°N is mostly land with a small ocean area so its contribution to the global average is rather small.

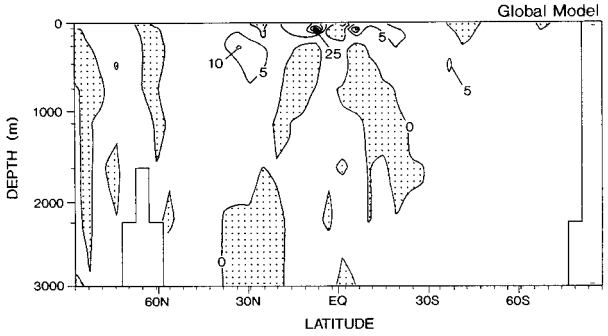


FIG. 8. Latitude vs depth section of zonally integrated APE dissipation in the standard global model due to horizontal mixing ($10^4$ erg cm$^{-2}$/s). A positive sign indicates that APE is being dissipated.

ing in Fig. 7 is completely negated by subtropical cooling.

Figure 7 shows that very little work is done by buoyancy forces in the Southern Ocean even though 15 Sv of deep water upwells to the surface in this area. Cooling in high southern latitudes generates APE at a rate of about 1 mW m$^{-2}$, but the cooling effect in this case is almost completely negated by the addition of ~0.5 m yr$^{-1}$ of fresh water by precipitation.

Figure 8 maps the dissipative effect of horizontal mixing in a latitude versus depth plot. The most intense APE dissipation occurs in the western boundary currents of the North Atlantic and North Pacific and in the North Equatorial Counter Current in the tropical Pacific. These are areas where second derivatives in the density field are especially large. It is noteworthy that very little APE dissipation occurs in the ACC even though model isopycnals slope up sharply in this area. This can be attributed to the fact that $\nabla_h^2\rho$ is not especially large in the ACC with respect to levels encountered in western boundary currents and the equatorial countercurrent.

### c. Sources and sinks of APE in the sector model

Figure 6 also summarizes the APE diagnostics for the sector model. The net source of APE due to surface buoyancy forces is $7.46 \times 10^{-6}$ erg cm$^{-3}$/s, more than three times larger per unit volume than the work done by buoyancy forces in the global model. This is mainly because the sector model has three times more vertical mixing in the upper kilometer where the mixing effect is most important.

The overall APE dissipation rate is $6.10 \times 10^{-6}$ erg cm$^{-3}$/s. Vertical mixing dissipates substantially more APE in the sector model, $4.42 \times 10^{-6}$ versus $1.10 \times 10^{-6}$ erg cm$^{-3}$/s, but again the overall work done by surface buoyancy forces exceeds the dissipation by mixing two to one. Horizontal mixing dissipates about one third less APE in the sector model, $1.68 \times 10^{-6}$ versus $2.44 \times 10^{-6}$ erg cm$^{-3}$/s.

The sum of APE sources and sinks, $S - B + (M + K)$, leaves an imbalance for the sector model of $0.58 \times 10^{-6}$ erg cm$^{-3}$/s, where the sources, $S$, exceed $-B + M + K$. The APE imbalance is 8% of the sources, about the same as in the global model. The advective terms, $H + V$, sum to a small negative number, $-0.26 \times 10^{-6}$ erg cm$^{-3}$/s, which is smaller than $-B$ by some $0.5 \times 10^{-6}$ units, but both $H + V$ and $-B$ are APE sinks in the sector model.

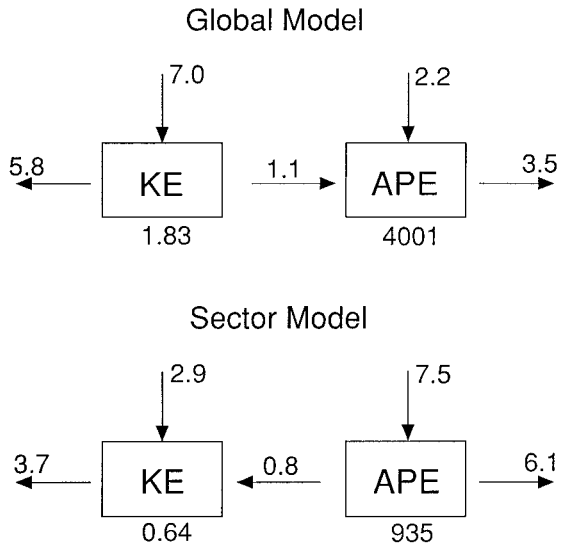


FIG. 9. Steady-state energy budgets in the standard global model (top) and the sector model S1.0 (bottom) (units $10^{-6}$ erg cm$^{-3}$/s). Average KE and APE per unit volume density is given below each box (erg cm$^{-3}$).

Figure 7 contrasts the way in which the work done by surface buoyancy forces is distributed latitudinally. The biggest difference is in the work done by surface heating to warm up upwelled deep water in the Tropics. Up to 150 W m$^{-2}$ of heat input is needed to warm up 13 Sv of deep water upwelling from below 1000 m (Fig. 2). There is no APE released by cooling in the subtropics in the sector model. Most of the upwelled water warmed up in the Tropics flows through the subtropics to be cooled in higher latitudes, where cooling adds to the overall APE generation.

Figure 9 summarizes the complete energy budgets for the two models. The relative roles of the wind forcing and buoyancy forcing are completely reversed. The winds do three times the work in the global model because wind stresses in the latitude band of the ACC add momentum to a swiftly moving current. Surface buoyancy forces do one-third of the work in the global model because the global model has less vertical mixing and less deep upwelling in low latitudes. The lion's share of the upwelling in the global model occurs south of the ACC core where surface buoyancy forces do not do any work to modify the upwelled water.

### d. Energy conversion

In some ways the most important difference between the global and sector models is the sign of the energy

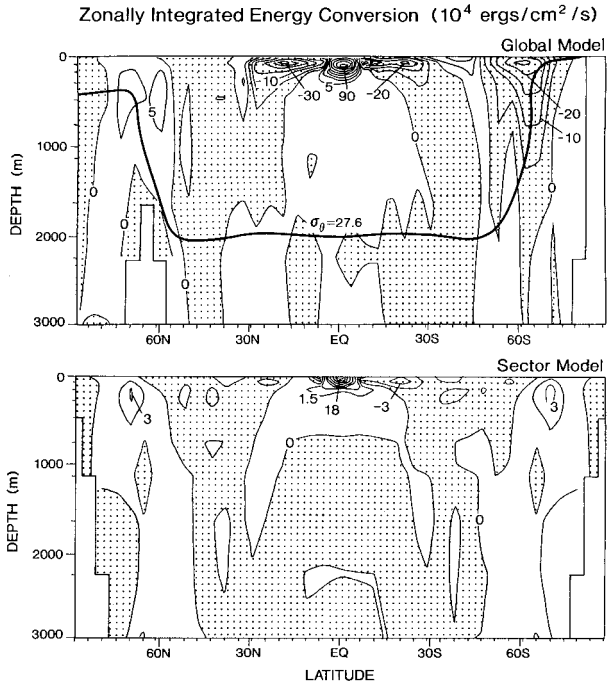


FIG. 10. Latitude × depth distribution of zonally integrated energy conversion in the standard global model (top) and the sector model S1.0 (bottom) ($10^4$ erg $cm^{-2}$/s). A positive sign indicates that APE is being converted to KE.

conversion term. Roughly 15% of the work done by winds in the global model is converted to APE, while 15% of the work done by buoyancy forces in the sector model is converted to KE. Figure 10 compares the latitudinal and vertical distribution of energy conversion between the global and sector models. Again, results are plotted as zonal integrals with units of $10^4$ erg $cm^{-2}$/s. As in Figs. 2 and 5, the contour interval is three times larger in the global model.

APE is generated from KE when the winds lift up dense water or pump down light water. Kinetic energy is released from the density field when dense water sinks or light water rises. The top panel of Fig. 10 shows that two regions of negative energy conversion (KE → APE) straddle an area of positive energy conversion (APE → KE) at the equator in the global model. Relatively light water pushed downward by Ekman convergence between 10° and 30° circulates into the equatorial region where it upwells back to the surface. The density of water circulated through this system is similar such that the drawdown of APE near the equator is nearly compensated by production of APE in the subtropics. The lower panel of Fig. 10 shows that the sector model is distinctly different. There is very little APE generation in the subtropics to compensate the drawdown near the equator. Most of the upwelling at the equator in the sector model is linked to sinking and cooling poleward of 60° in both hemispheres where the sinking also acts to draw energy out of the density field.

The biggest difference between the global and sector models is the large area of negative energy conversion (APE generation) centered on 60°S in the global model. This area is south of the band of maximum kinetic energy in Fig. 5, that is, just south of the ACC core. Here the divergence in the wind stress field lifts 15–20 Sv of 1°–2°C water from depths as great as 3000 m toward the surface. Upwelling of such dense water from these depths increases horizontal density differences throughout the ocean's interior and counteracts a net positive energy conversion elsewhere. The work done by the winds to lift dense water south of the ACC amounts to 25% of global KE generation, or $1.9 \times 10^{-6}$ erg $cm^{-3}$/s in the units of Fig. 9. This input of energy amounts to 5 m W $m^{-2}$ per unit area over the 50°–70°S latitude band. It is comparable to the work done by buoyancy forces in the Tropics (Fig. 7) and it greatly exceeds the work done by buoyancy forces in the Southern Ocean. Ivchenko et al. (1997) report that upwelling south of the ACC in the Fine Resolution Antarctic Model (FRAM) is also a large APE source of about the same magnitude.

New deep water forming in the global model's North Atlantic has an average potential density of 27.6. Included in Fig. 10 is a dashed line that shows the zonally averaged depth of the $\sigma_\theta = 27.6$ isopycnal. The 27.6 isopycnal directly connects a region of dense sinking in the North Atlantic with the large area of dense upwelling in the south. This shows that the model's North Atlantic Deep Water travels nearly from pole to pole through the interior and upwells to the surface south of the ACC with essentially no density modification by mixing. Sinking of North Atlantic Deep Water in the model releases energy from the density field as expected, but this loss of APE is more than compensated for by an increase in APE when water with this density is raised to the surface in the south.

### *e. The ocean energy analysis of Oort et al. (1994)*

Figure 11 shows a comparison of the energy analysis derived by OAP94 and that derived here from the global model. Sources and sinks in the OAP94 results (reported in mW $m^{-2}$) have been divided by 4000 m in order that both sets of results have units of energy change per unit volume per second. Both the OAP94 energy budget and the budget from the global model appear to be in balance, but they balance in very different ways. Overall the sources and sinks of KE and APE derived by OAP94 are substantially larger. The work done by winds is a factor of 2 larger and the work done by buoyancy forces is 4.5 times larger in the OAP94 analysis. Energy conversion in OAP94 is some 2.5 times larger and directed toward KE rather than toward APE.

The difference in wind work is not due to wind stresses since both OAP94 and the global model use stresses derived from the same dataset (Hellerman and Rosenstein 1983). The difference is mainly accounted for by

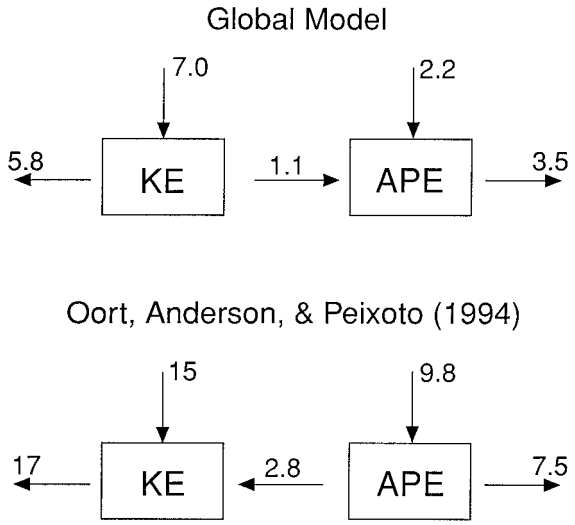


FIG. 11. Comparison of energy sources and sinks in the standard global model (top) and in the OAP94 analysis (bottom) (units $10^{-6}$ erg $cm^{-3}/s$). Sources and sinks reported by OAP94 per unit ocean area are given here per unit volume after dividing by 4000 m.

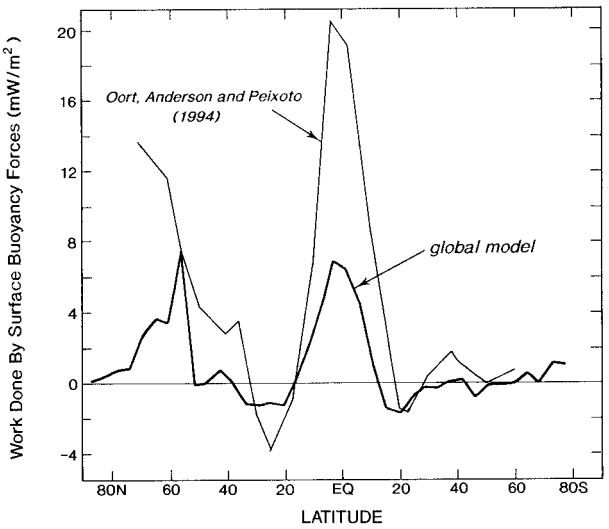


FIG. 12. Work done by surface buoyancy forces in the standard global model and in the analysis of OAP94 plotted as a function of latitude. Results are simple zonal averages ($10^{-3}$ W $m^{-2}$) as in Fig. 7.

the fact that observed surface currents derived from ship drift used in OAP94 are more than two times faster than model currents in many places.

The work done by surface buoyancy forces in OAP94 is $9.8 \times 10^{-6}$ erg $cm^{-3}/s$ versus $2.2 \times 10^{-6}$ erg $cm^{-3}/s$ in the global model. This difference is not due to heat and salt fluxes across the air–sea interface. These tend to be similar in both the model and the OAP94 analysis—both show 50–100 W $m^{-2}$ heat fluxes in the equatorial Pacific and 0.5–1.0 m $yr^{-1}$ of net evaporation in the subtropical gyres. The main difference between the two figures comes from the stability factor, which appears in the denominator of the APE expression in Eq. (4).

The stability factor used in the Lorenz approximation scales the work being done when heat and freshwater fluxes alter the density of water in the surface layer. Ideally, it would be a horizontal average of the stability at the base of all the ocean's mixed layers. The stability factor used by OAP94, 0.0037 kg $m^{-4}$, is derived from the average density difference across 10 m in the Levitus (1982) data. This stability is unrealistically low because 10 m is well within the mixed layer in most places. The stability factor derived from the global model, 0.0087 kg $m^{-4}$, is the average stability at the *base* of the model's first layer at 51 m. Figure 12 compares the work done by heating/cooling plus freshening/salinification as derived by OAP94 and the global model. The OAP94 curve has the same features as the model curve, only the absolute magnitude of the numbers is exaggerated because of the small stability factor.

OAP94's energy conversion term is derived from published overturning rates for the North Atlantic derived from models, but OAP94 assume that high-latitude sinking is balanced entirely by low-latitude upwelling as in the sector model. They assume further that energy conversion rates for the Northern Hemisphere hold for the Southern Hemisphere as well. These assumptions lead to an APE sink of $2.8 \times 10^{-6}$ erg $cm^{-3}/s$ due to energy conversion that has the opposite sign and is nearly three times larger than the energy conversion in the global model. APE dissipation in OAP94, at $7.5 \times 10^{-6}$ erg $cm^{-3}/s$, is also very large and is more than twice the APE dissipation in the global model. The OAP94 figure is based on a sketchy calculation to assess the rate of dissipation due to horizontal advection. Our analysis shows that APE dissipation arises only from the effects of mixing and that these sinks are relatively small.

The OAP94 energy budget appears to be in balance with $\sim 10 \times 10^{-6}$ erg $cm^{-3}/s$ of APE production due to surface buoyancy forces. But an APE source of this magnitude is only possible with large sinks due to energy conversion and dissipation. Our model-based energy analysis suggests that energy conversion is not a sink for APE and that the overall dissipation rate is rather small.

## 4. Energy and circulation as a function of vertical mixing

The sector model of Bryan (1987), with its zonal extent of 60° of longitude, was designed to simulate the thermohaline circulation in the Atlantic Ocean. Two circulation targets define this circulation, the strength of the deep western boundary current carrying North Atlantic Deep Water southward along the eastern margin of North America ($\sim$15 Sv), and the northward transport of heat across 25°N ($\sim 1 \times 10^{15}$ W). Bryan's sector model needs a very high vertical mixing coefficient, $>2.5$ $cm^2$ $s^{-1}$, to actually hit these targets. The global

TABLE 3. Additional model results.

| Model | KE | APE | Work done by wind ($10^{-6}$ erg cm$^{-3}$/s) | Work done by buoyancy forces ($10^{-6}$ erg cm$^{-3}$/s) | ACC (Sv) | Low-latitude upwelling across 1350 m (Sv) | Atlantic outflow at 31°S (Sv) | Heat transport across 31°N ($10^{15}$W) Global | Heat transport across 31°N ($10^{15}$W) Atlantic |
|---|---|---|---|---|---|---|---|---|---|
| | | | | Sector | | | | | |
| S0.1 | 0.38 | 478 | 2.48 | 1.12 | | 1.4 | | 0.119 | |
| S0.5 | 0.48 | 678 | 2.52 | 4.01 | | 7.9 | | 0.303 | |
| **S1.0** | **0.67** | **970** | **2.87** | **7.46** | | **13.2** | | **0.448** | |
| S2.5 | 1.16 | 1532 | 2.93 | 17.0 | | 26.2 | | 0.816 | |
| Asymmetric | 0.82 | 1031 | 2.94 | 6.46 | | 12.6 | | 0.923 | |
| | | | | Global | | | | | |
| **Standard** | **1.83** | **4001** | **7.01** | **2.18** | **180** | **9.0** | **11.1** | **0.958** | **0.657** |
| G0.5 | 2.19 | 4670 | 7.32 | 3.30 | 214 | 14.6 | 12.7 | 1.092 | 0.751 |
| G1.0 | 3.05 | 6683 | 7.89 | 5.97 | 304 | 26.9 | 17.3 | 1.420 | 1.005 |
| G2.5 | 4.92 | 9414 | 8.57 | 14.3 | 407 | 59.4 | 21.5 | 1.816 | 1.237 |
| Standard − no winds | 0.28 | 1931 | 0 | 2.01 | 84 | 8.6 | 4.3 | 0.420 | 0.299 |
| N0.1 | 0.07 | 1094 | 0 | 0.79 | 36 | 3.7 | 2.2 | 0.233 | 0.167 |
| N0.5 | 0.50 | 2311 | 0 | 3.14 | 124 | 11.9 | 6.7 | 0.599 | 0.424 |
| N1.0 | 1.26 | 5238 | 0 | 5.94 | 218 | 21.5 | 10.4 | 0.912 | 0.635 |
| G30S | 0.97 | 2510 | 3.16 | 2.27 | 91 | 9.4 | 4.3 | 0.661 | 0.431 |
| Nonsinking | 2.19 | 4462 | 7.45 | 2.12 | 227 | 5.5 | 1.0 | 0.549 | 0.220 |

model, on the other hand, comes fairly close to hitting the Atlantic targets with much less vertical mixing.

The global model hits the Atlantic circulation targets with relatively little vertical mixing because it contains a distinct variety of overturning that the sector model does not have, namely a transequatorial ''conveyor'' circulation that transports warm South Atlantic water northward across the equator near the surface and cold North Atlantic water out of the Atlantic at depth (Broecker 1991). This is a curious result: If the global model with a strong conveyor manages to hit the Atlantic circulation targets with relatively little vertical mixing, then the conveyor circulation must not be very dependent on vertical mixing.

In this section, a series of global and sector models is run out with the same vertical mixing coefficients, 0.1, 0.5, 1.0, and 2.5 cm$^2$ s$^{-1}$, constant with depth, used by F. Bryan (1987). Energy and circulation diagnostics from these models are then plotted as a function of vertical mixing. Simple linear trends emerge for mixing rates between 0.1 and 1.0 cm$^2$ s$^{-1}$. These diagnostics show that a strong outflow of deep water from the North Atlantic persists at the limit of no vertical mixing with very little energy input from buoyancy forces.

A description of the new global and sector models is given in Table 1. Tables 2 and 3 give the energy balance and selected circulation diagnostics. The new sector models are identified as S0.1, S0.5, S1.0, and S2.5, where S1.0 is the sector model from the first part of the paper. Wind-forced global models are identified as G0.1, G0.5, G1.0, and G2.5. A set of global models has also been run out with no wind forcing. These are identified as N0.1, N0.5, and N1.0. Three additional global models were run out with the Bryan and Lewis (1979) vertical mixing coefficients, which vary with depth from 0.3 to 1.3 cm$^2$ s$^{-1}$. These are the standard global model itself, the standard model without wind forcing (''standard-no winds''), and a model with wind forcing north of 30°S only (''G30S''). Differences between the standard model and G30S are due to the winds south of 30°S that drive the ACC. Selected results from Tables 2 and 3 are plotted as a function of vertical mixing in Figs. 13–15.

The Bryan and Lewis mixing coefficients are close to the lower limit that can be tolerated with the grid resolution used in the global models. Mixing coefficients smaller than 0.3 cm$^2$ s$^{-1}$ in the upper kilometer lead to numerical errors. Thus, the G0.1 results are not reliable and none are tabulated in Tables 2 and 3. Global models without winds, or sector models without an ACC, on the other hand, can be run successfully with smaller mixing coefficients, for example, N0.1, S0.1. The higher mixing coefficients applied by Bryan and Lewis in the deep ocean do not seem to be important energetically. When energy and circulation diagnostics from the models using the Bryan and Lewis mixing are plotted in Figs. 13–15 at 0.3 cm$^2$/s they fall on the same trend lines as results from models with constant mixing coefficients.

Figure 13 shows the globally averaged APE and KE and the strength of the ACC for all the models in Table 1 plotted as a function of vertical mixing coefficient. Diagnostics from the global models and the sector models plot along significantly different slopes. Sector model results (plus signs) plot along a shallow linear trend along the bottom part of each figure, while the global results plot along much steeper trends. There is a large vertical offset between the wind-forced global models (solid circles) and the global models without winds

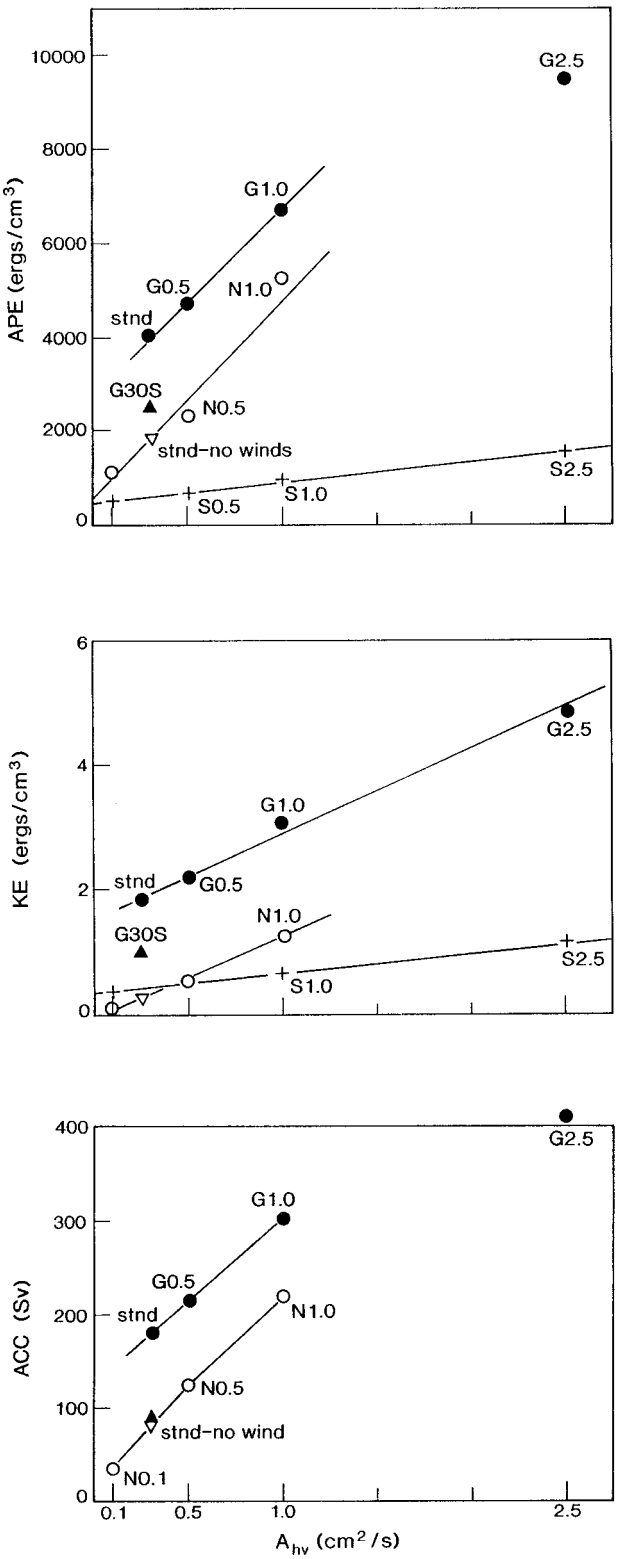


FIG. 13. Globally averaged APE (top) and KE (middle), and ACC strength (bottom) plotted as a function of vertical mixing coefficient, $A_{hv}$, for the global and sector models listed in Table 1. Results from the standard model, standard − no winds, and G30S, are plotted at $A_{hv} = 0.3$ cm$^2$ s$^{-1}$ even though higher mixing rates are used at depth.

(open circles), which is more-or-less constant over vertical mixing rates between 0.1 and 1.0 cm$^2$ s$^{-1}$. The constant offset shows that the wind contribution is about the same at all mixing rates.

Two features are of particular interest. First, the wind effect on APE and KE is much larger in the presence of a circumpolar current than the combined wind and buoyancy effects in any of the sector models. The wind effect in the global model comes disproportionally from the winds south of 30°S that drive the ACC. The effect of winds north of 30°S is given by the offset between G30S (solid upright triangle—winds north of 30°S only) and the no-winds model (open upside down triangle). The effect of winds south of 30°S is given by the offset between G30S and the full-wind standard model. Winds south of 30°S account for roughly half of the wind effect in global KE and about three-quarters of the wind effect in APE (some 1500 erg cm$^{-3}$). Winds south of 30°S account for virtually all the wind offset in ACC strength, as one would expect.

Second, modest amounts of vertical mixing ($\geq$0.5 cm$^2$ s$^{-1}$) drive a strong ACC (>100 Sv) through the circumpolar channel in the absence of winds. Similar results are reported by Cai and Baines (1996). Vertical mixing operating in the presence of an open circumpolar channel causes isotherms in the interior to be depressed in relation to the cold water around Antarctica. These density differences are able to drive a strong eastward flow through the channel when there are topographic obstacles at depth. The zonal flow is linked to a weak overturning circulation across the channel, which converts APE in the density field into KE in the zonal flow (see discussion).

Figure 14 shows selected overturning diagnostics as a function of vertical mixing. The top panel shows the volume of deep water upwelled across 1000 m between 31°S and 31°N. Unlike the results in Fig. 13, the trend in deep upwelling extrapolates to the origin for each set of models. This indicates that there is no deep upwelling in low latitudes at the limit of no vertical mixing, as in F. Bryan (1987). There is also no wind effect on the upwelling of deep water in low latitudes.

The middle panel of Fig. 14 shows the strength of the conveyor circulation in the global models as a function of vertical mixing. The conveyor strength is defined here as the outflow of deep water of North Atlantic origin across 31°S. As in Fig. 13, there is a substantial offset between the wind-forced and no-winds cases, indicating that the conveyor responds strongly to the wind forcing. The wind effect is nearly 10 Sv and it appears to be independent of vertical mixing. The slope between the Atlantic outflow and vertical mixing is fairly shallow such that the wind effect accounts for most of the Atlantic outflow for vertical mixing rates less than 1.0 cm$^2$ s$^{-1}$. The G30S result plots right on the no-winds trend. This indicates that only the winds south of 30°S, that is, the winds that drive the ACC, enhance the Atlantic outflow. Since there is no deep upwelling in low lati-

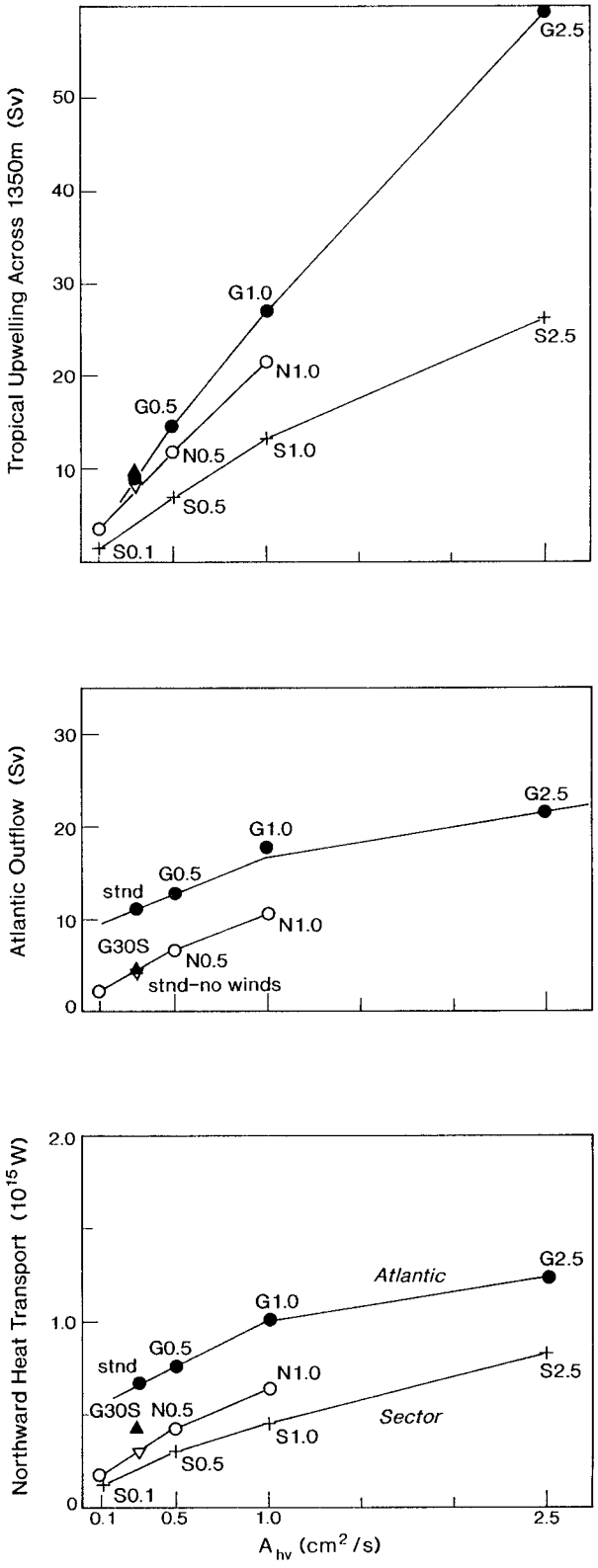


FIG. 14. Low-latitude upwelling across 1350 m (31°N–31°S) (top), Atlantic outflow across 31°S (middle), and northward Atlantic heat transport at 31°N (bottom) plotted as a function of vertical mixing coefficient, $A_{hv}$, for the models listed in Table 1.

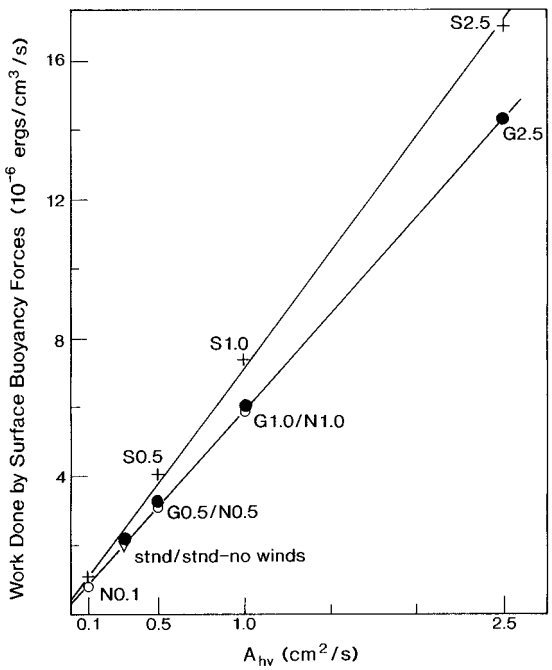


FIG. 15. Work done by surface buoyancy forces as a function of vertical mixing coefficient, $A_{hv}$, for the models in Table 1 (units $10^{-6}$ erg cm$^{-3}$/s).

tudes at the limit of no mixing, yet a strong conveyor circulation still exists, all the upwelling that closes the conveyor circulation must occur elsewhere, presumably south of the ACC.

The bottom panel of Fig. 14 gives the northward heat transport at 31°N in the Atlantic basin. Sector model heat transports are shown for comparison. The heat transport in the sector models and in the Atlantic basin of the global no-wind models are similar at the same level of vertical mixing. Here again, there is a substantial upward offset in heat transport for the wind-forced global models. Heat transport in the no-wind and sector models nearly vanishes with no mixing, whereas the heat transport in the wind-forced global models is still about $0.5 \times 10^{15}$ W.

### *Work done by wind forces and buoyancy forces at the limit of no mixing*

Figure 15 shows the work done by surface buoyancy forces in the same format as Figs. 13 and 14. In this plot, results from the global models and sector models are all quite similar at a given level of vertical mixing. Global results with and without winds plot along the same trend such that there is no extra work done by buoyancy forces in response to the winds. Extrapolating the trends in Fig. 15 to the limit of zero mixing yields a small $y$ intercept of about $0.40 \times 10^{-6}$ erg cm$^{-3}$/s in both cases, which is not much different from zero given the errors in this analysis. For the most part, the work

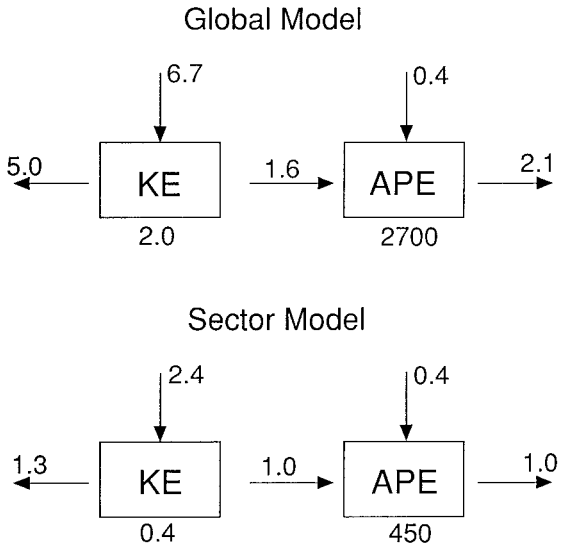


FIG. 16. Projected energy budgets in the global model (top) and the sector model (bottom) at the limit of zero vertical mixing ($10^{-6}$ erg cm$^{-3}$/s). Average KE and APE per unit volume is given below each box (erg cm$^{-3}$).

done by buoyancy forces scales one-to-one with the upwelling of deep water in low latitudes. According to Fig. 15, the wind-driven component of the Atlantic outflow manages to operate with very little work done by surface buoyancy forces.

In Fig. 16 we attempt to assess the energy budgets in the global and sector models at the limit of no vertical mixing. This has been done by graphically extrapolating all the terms in the energy budget to zero mixing as was done in Figs. 13–15. Both budgets are roughly in balance with the surface buoyancy forces contributing 0.40 $\times$ $10^{-6}$ ergs/cm$^3$/s, that is, the $y$ intercept in Fig. 15. Not surprisingly, both energy budgets show a net conversion of KE to APE. The global model has 60% more APE production due to energy conversion and two times more APE dissipation than the sector model. The biggest differences are reflected in the standing stocks of KE and APE: the global model has five times more KE and six times more APE than the sector model with essentially the same forcing.

## 5. Discussion

One is hard pressed to find evidence that any deep upwelling is taking place in low latitudes, much less 10 Sv or more (Toggweiler and Samuels 1993). According to the results in the previous section, there is very little work done by surface buoyancy forces if there is no upwelling of deep water in low latitudes. The question to be addressed here is whether the overturning in the real world can operate with a small input of energy from buoyancy forces. This seems to defy common sense because the ocean's large-scale circulation clearly involves much heating and cooling and an important role for salinity differences (Bryan 1986; Broecker 1991).

Two points are made below. First, it is fairly easy to show that the existence of a gap between South America and Antarctica dominates the thermal structure of the ocean's interior. A wind-driven ACC flowing through the gap can maintain the observed thermal structure with no energy input from vertical mixing and surface buoyancy forces. Second, while the cooling of surface waters in the North Atlantic appears to be a major driving force for the Atlantic conveyor, our energy perspective suggests otherwise. We find that most of the heating and cooling associated with the conveyor circulation is a passive response to the overturning and is not part of the forcing.

### *a. The ACC and the ocean's thermal structure*

Figure 17 shows latitude by depth sections of zonally averaged temperatures in four different cases. The top panel shows the observed temperature structure from the Levitus (1982) climatology. The second panel shows zonally averaged temperatures for the sector model S1.0. The third and fourth panels show zonally averaged temperatures from the no-winds and wind-forced versions of the standard global model. The thermal structure in the sector model is distinctly different from the thermal structure in the Levitus climatology or the two global models. The sector model has a tight packing of isotherms above 1000 m but has virtually no temperature structure and no stratification below 1000 m. The temperature structure in both global models extends continuously into the deep ocean as in the Levitus observations.

Many studies have attempted to link the ocean's thermal structure below 1000 m with vertical mixing coefficients of order 1 cm$^2$ s$^{-1}$ (e.g., Munk 1966; Cummins et al. 1990). However, this recipe does not explain the results here: the sector model in Fig. 17 was run with a uniform vertical mixing coefficient of 1.0 cm$^2$ s$^{-1}$ and it has essentially no thermal structure below 1000 m. Basically, the meridional overturning circulation in a closed basin is a very efficient mechanism for extracting energy from the density field. Overturning in the sector model converts APE into KE by pushing isotherms up into the upper kilometer and by filling the interior with uniformly cold water. The temperature structure attributed by previous studies to vertical mixing is really due to the gap between South America and Antarctica and the existence of a continuous circumpolar channel.

The thermal structure in the real world and in the global models in Fig. 17 is characterized by 0°C water up against Antarctica and substantially warmer water at all depths north of the circumpolar channel. This temperature difference reveals the presence of a substantial amount of APE throughout the interior. These deep temperature differences exist because the circumpolar channel blocks the kind of meridional overturning seen in

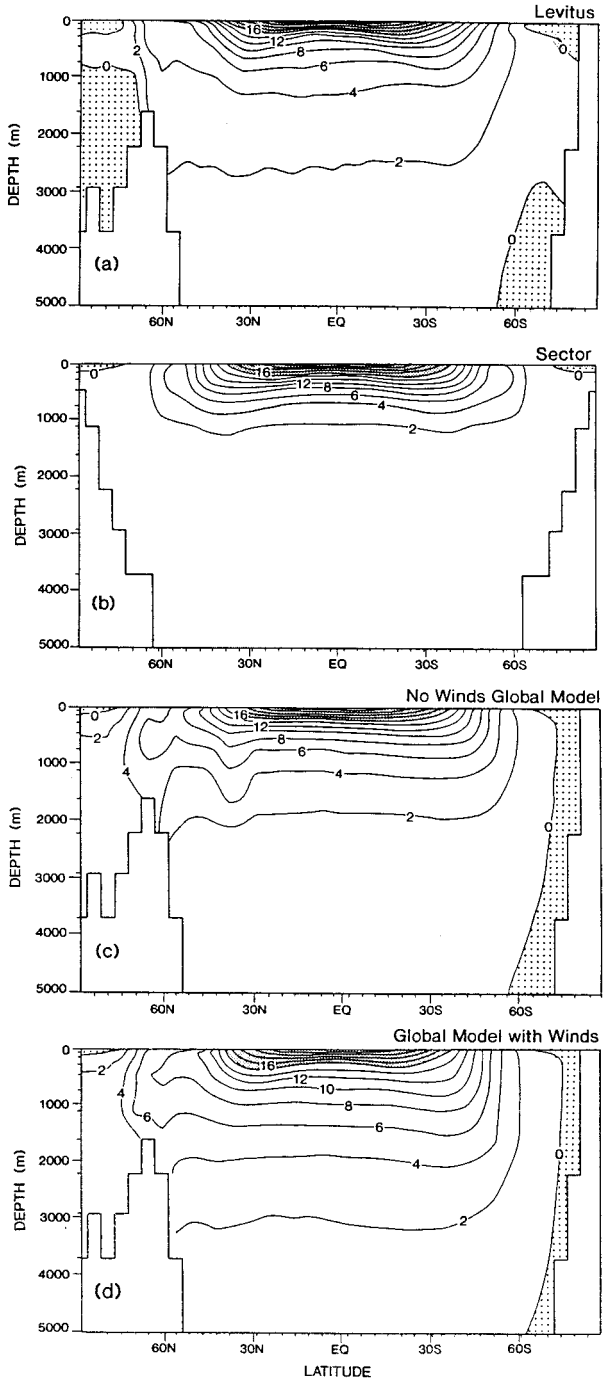


FIG. 17. Comparison of zonally averaged temperatures in (a) the Levitus (1982) climatology, (b) the sector model S1.0, (c) the standard − no winds global model, and (d) the standard global model with winds.

the sector model. Energy put into the density field, either by winds or buoyancy forces, is not so easily drained away.

In the absence of winds, vertical mixing and low latitude heating warm the interior in relation to the 0°C temperatures in the south. Density differences across the circumpolar channel drive an eastward zonal flow and produce an attenuated meridional overturning, which develops in tandem with the zonal flow. Frictional dissipation in the zonal flow provides for an ageostrophic southward flow in the interior, which allows the dense water around Antarctica to leak out to the north at depth (Cai and Baines 1996). This weaker variety of overturning converts APE in the density field into KE in the ACC. Since the ACC is essentially a zonal current with minimal contact with land, it becomes quite large (84 Sv) before it generates enough friction to dissipate the energy put into the density field by vertical mixing and low-latitude heating.

Vertical mixing can produce a surprisingly energetic ocean in the presence of a circumpolar channel. The 84-Sv zonal flow in the standard no-winds model is a significant fraction of the ACC flow in the real world, ~130 Sv (Whitworth and Peterson 1985). The thermal structure in the standard no-winds model is similar to the observed structure. The 4° and 6° isotherms in Fig. 17 are close to Levitus depths; the 2° isotherm is a bit too shallow. All the no-winds global models in this paper maintain relatively high standing stocks of APE with no energy input from the winds at all (Table 3).

In the presence of winds, energy flows directly into the density field via Ekman pumping. The effect of the winds and the effect of vertical mixing combine in a fairly linear way to strengthen the ACC and to depress isotherms north of the ACC. Figure 17 shows that isotherms in the standard wind-forced global model are hundreds of meters deeper than in the no-winds model. In fact, isotherms in the wind-forced model are much deeper than the Levitus isotherms and the ACC is too strong (180 Sv). This indicates that the combined effect of the winds and vertical mixing produces too much APE and too much zonal flow.

Extrapolation of the trends in Fig. 13 to zero mixing shows that the standard wind-forced model would have roughly the right thermal structure (~2500 ergs $cm^{-3}$) and ACC strength (~125 Sv) if it could be run without vertical mixing. This means that either the wind effect or the vertical mixing effect by themselves can reproduce the observed thermal structure and ACC strength in the presence of a circumpolar channel. Granted that there are large uncertainties about the actual magnitudes of both effects, we would argue that the thermal structure in the real world is probably derived without much input from vertical mixing, that is, with the winds acting alone. We say this because vertical mixing is invariably linked to a large volume of deep upwelling in low latitudes, which is not observed.

Figure 18 illustrates in a slightly different way how the effect of the winds and the effect of vertical mixing overlap in the presence of a circumpolar channel. Figure 18 shows how model APE is distributed in the vertical. APE for each model is plotted as a simple vertical profile. The top panel shows results from the four sector

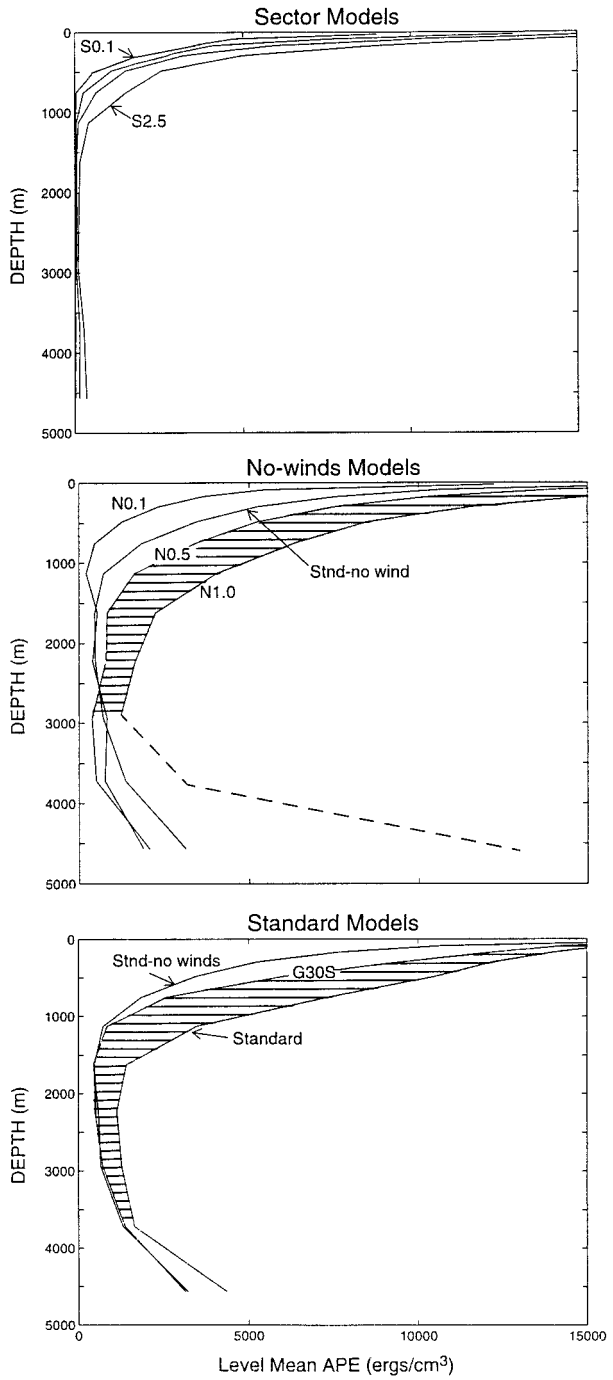


FIG. 18. Level mean APE (erg $cm^{-3}$) as a function of depth for the sector models (top), no-winds global models (middle), and the standard, standard − no winds, and G30S models (bottom).

models. Basically all the APE in the sector models is found above 1000 m as one would infer from the thermal structure in Fig. 17. The deep interior is filled with uniformly cold water and has no APE even with large mixing rates. The middle panel shows the vertical APE distribution from the four no-winds global models. With an open circumpolar channel, there are substantial nonzero levels of APE throughout the interior, even with low levels of vertical mixing.

The bottom panel of Fig. 18 shows the effect of systematically switching on the winds. First, results from the standard no-winds model are repeated from the middle panel. Then, the winds north of 30°S are added (G30S). The winds south of 30°S are added in the fully forced standard model. Switching on the winds north of 30°S increases APE only in the upper kilometer, as one might expect. The effect of the winds south of 30°S is more substantial and extends all the way to the bottom. The change in APE associated with an increase in vertical mixing from 0.5 to 1.0 $cm^2\ s^{-1}$ in the middle panel has been hatched in order that it can be directly compared with the change in APE associated with the winds south of 30°S. Winds south of 30°S increase APE and enhance the deep thermal structure to roughly the same extent as an 0.5 $cm^2\ s^{-1}$ increase in vertical mixing.

The model results in Fig. 17 suggest that the ACC keeps most all of the water in the ocean's interior relatively warm and less dense than it would be otherwise. This effect was first illustrated in the pioneering study of Cox (1989). Cox showed that an ocean without a circumpolar channel and without winds should be filled with uniformly cold water from the Southern Ocean. When a circumpolar channel is opened, the interior north of the channel becomes warmer and more stratified while the influence of cold southern waters is dramatically reduced. When winds are turned on, Cox's interior becomes even warmer as various intermediate waters and deep water from the Northern Hemisphere fill the void left by retreating southern-source waters. Vertical mixing rates and the volume of upwelling in low latitudes are constant across Cox's set of experiments, so these particular changes in thermal structure have little to do with changes in the surface buoyancy forcing. It is really the channel itself that warms the interior: the channel blocks the meridional overturning, which would otherwise flatten north–south temperature differences, and it provides a conduit for the ACC through which the winds directly enhance north–south temperature differences.

The warm interior isotherms in Fig. 17 extend all the way up into the high latitudes of the North Atlantic where new deep water flows over the Icelandic sills (~600 m) and sinks to form North Atlantic Deep Water (NADW). The presence of relatively warm water in the interior south of Iceland significantly enhances the density contrast between new deep water and ambient deep water. Thus, the channel and wind effects in the south make it easier for deep water to form in the Northern Hemisphere. They make substantially more energy available to the overturning when NADW sinks.

In summary, the starting point for understanding the ocean's density and thermal structure is the existence of a circumpolar channel. Of course, the channel does not put any energy into the density field by itself. Something else, either vertical mixing or energy input by the winds, is needed. The energy input for maintaining the ocean's

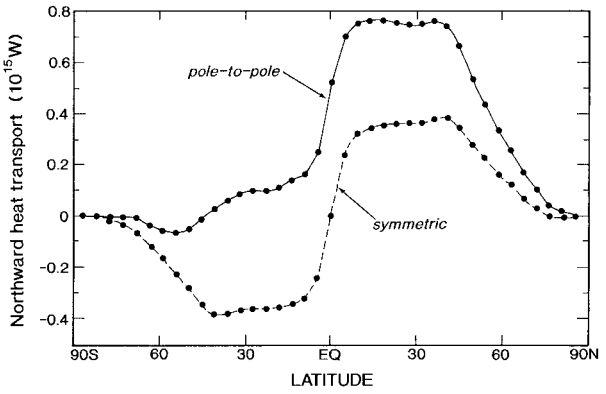


FIG. 19. Comparison of the northward heat transport in the F. Bryan (1986) sector model between pole-to-pole and equatorially symmetric states of the circulation ($10^{15}$ W). Reproduced from F. Bryan (1986).

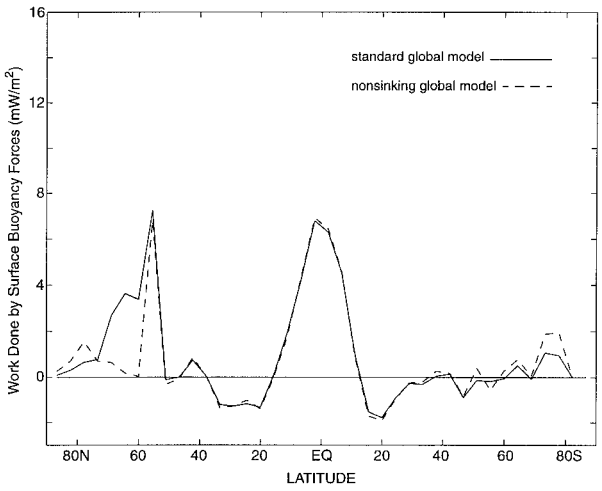


FIG. 20. Work done by surface buoyancy forces as a function of latitude in the standard global model with active sinking in the North Atlantic (solid line) and the nonsinking global model (dashed line). Results are simple zonal averages as in Fig. 7 ($10^{-3}$ W m$^{-2}$).

density structure could come exclusively from the winds driving the ACC. A background level of vertical mixing may exist in the ocean's interior, but it is not required to account for the large-scale thermal structure.

### *b. Role of buoyancy forces in the conveyor circulation*

Using the same sector model used here, Bryan (1986) illustrated how an equatorially symmetric circulation with two separate hemispheric cells (as in Fig. 2) reverts to a single pole-to-pole overturning when north–south asymmetries are present in the surface salinity forcing. This conveyor-like circulation dramatically increases the northward heat transport when surface waters are saltier in the Northern Hemisphere. Figure 19 reproduces the northward heat transport in Bryan's equatorially symmetric case (bottom curve) and the pole-to-pole case (top curve) as a funtion of latitude. The northward heat transport in the pole-to-pole case is larger by a factor of 2.

The pole-to-pole circulation of Bryan (1986) has been reproduced here in both the global and sector models. This change in the sector model was brought about by replacing the surface restoring of salinity with the two-dimensional salt flux field implied by the restoring operation in S1.0. After several hundred years of integration, the meridional overturning in the new model spontaneously flips into an asymmetric pole-to-pole circulation (as reported in Bryan 1986). Surface salinities drop by 3 ppt at 50°S and increase by 3 ppt at 50°N. Deep salinities increase on average by 0.15 ppt. A similar transition was brought about in the global model by running out a new model in which the surface salinities being restored to in the North Atlantic were reduced to suppress sinking. The increase in Atlantic sinking between this ''nonsinking'' global model and the actively sinking standard case (14 Sv) is similar to the increased northern sinking in the asymmetric sector model (12 Sv). Globally averaged energy and circulation diagnostics for the nonsinking global model and the equatorially asymmetric sector model are included in Tables 2 and 3.

Figure 20 compares the work done by surface buoyancy forces in the nonsinking and actively sinking versions of the global model. It shows, somewhat suprisingly, that switching on the conveyor circulation and tripling the northward heat transport in the actively sinking model involves very little change in the work done by surface buoyancy forces. The only substantial difference between the two curves in Fig. 20 is at latitudes between 60° and 70°N where sinking occurs. Since model grid rows in this latitude band contain relatively few ocean grid cells, the changes between 60° and 70°N are a small effect globally. The average work done by surface buoyancy forces is only 3% larger in the active-sinking case ($2.18 \times 10^{-6}$ vs $2.12 \times 10^{-6}$ ergs cm$^{-3}$/s). The work done by buoyancy forces in the asymmetric sector model is 13% lower than in the equatorially symmetric case.[2]

To understand why this might be true, a distinction must be made about where heat is taken up in the conveyor circulation. The two heat transport curves for the pole-to-pole and equatorially symmetric circulations in Fig. 19 are parallel as they cross the equator. This means that the heat uptake at the equator, that is, the change in heat transport per unit latitude, is the same in the equatorially symmetric and asymmetric circulations. Switching on the pole-to-pole or conveyor circulations

[2] Certain aspects of the comparison between energy budgets in the symmetric and asymmetric versions of the sector model do not make sense. More APE is converted to KE via energy conversion in the asymmetric model, and less APE is generated by surface buoyancy forces, yet the standing stock of APE in the asymmetric model is supposedly larger. Comparing APE diagnostics at the 10% level in such different models may be pushing the Lorenz approximation too far.

does not alter the heat uptake in the Tropics. Figure 20 shows that the same effect is at work in the active-sinking global model. Switching on the conveyor has no effect on the work done by surface buoyancy forces in low latitudes.

The pole-to-pole heat transport curve in Fig. 19 slopes upward to the north in relation to the lower curve throughout the Southern Hemisphere. It slopes downward in relation to the lower curve throughout the Northern Hemisphere. This means that heat given up by the ocean in the Northern Hemisphere is taken up from the atmosphere at comparable latitudes in the Southern Hemisphere. More specifically, for every increment of heat given up at one density in the north, there is an increment of heat taken up at a similar density in the south. In energy terms, the work associated with enhanced cooling in the north is negated one-for-one by the effect of enhanced heating in the south. With no extra heating in the Tropics, the surface buoyancy forces do no extra work to maintain the pole-to-pole circulation. Most of the enhanced northward heat transport associated with the conveyor is a passive response to an overturning that moves Southern Hemisphere heat across the equator to the Northern Hemisphere.

The main energy change associated with switching on the conveyor is a release of potential energy from the density field. Higher surface salinities and enhanced sinking in the North Atlantic make the deep ocean saltier and denser. Individual density surfaces become shallower while the thermocline becomes flatter and thinner. Figure 21 attempts to illustrate these changes in the two sets of models. The top panel shows the change in vertical stability as a function of depth between the symmetric and asymmetric states of the sector model. (Vertical stability is used here as a more robust surrogate for APE.) The transition between states is associated with a change from a less stable (symmetric) to a more stable (asymmetric) density field throughout the upper 2000 m. The bottom panel of Fig. 21 shows the actual change in APE between the nonsinking and active-sinking states of the global model. The active-sinking state has significantly less APE between 500 and 2000 m than the nonsinking state.

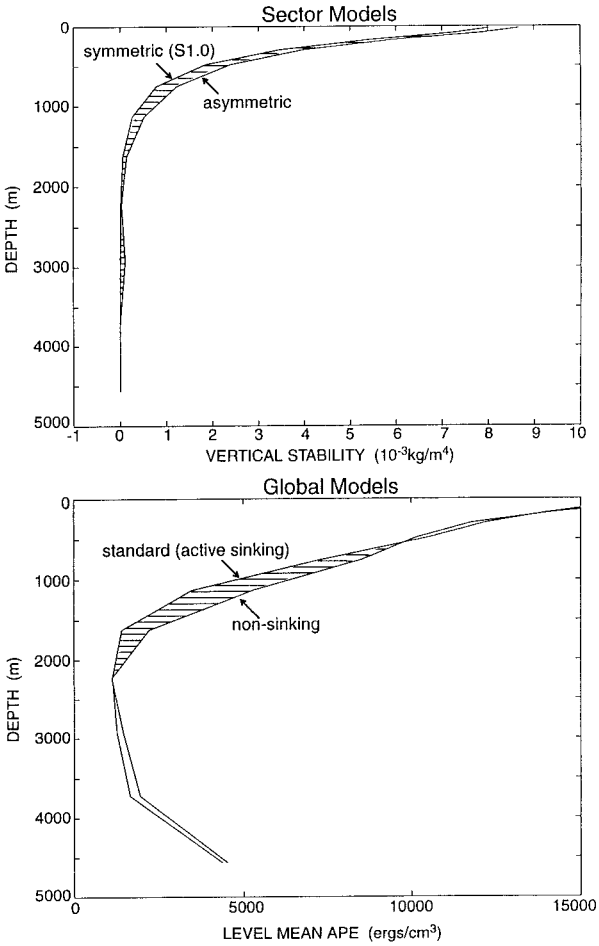


FIG. 21. Mean vertical stability ($10^{-3}$ kg m$^{-4}$) as a function of depth for the symmetric sector model S1.0 and its asymmetric counterpart (top). Level mean APE (erg cm$^{-3}$) as a function of depth between the nonsinking and standard (active sinking) global models (bottom). The asymmetric sector model with pole-to-pole overturning and the global model with active sinking in the North Atlantic have more stability and less APE in the interior.

These results are consistent with the idea presented in Rooth (1982) and Bryan (1986) that an equatorially symmetric circulation in the sector model is unstable. Slightly higher salinities in one hemisphere rapidly bring about a transition to the energetically favored state through a release of potential energy in the unstable mode. In the same vein, the density field in the nonsinking global model is unstable to higher salinities in the sinking region.

The surface salinities that initiate sinking in the North Atlantic are due to the transport of salty water from low latitudes. A weak local effect in high latitudes (i.e., a small excess of precipitation over evaporation) allows subtropical salinities to persist into the sinking region. High surface salinities do work on the system indirectly by allowing high-latitude cooling to extract more buoyancy. We find that the enhanced cooling effect associated with high surface salinities is a small effect buried within the errors of our energy analysis. This small effect is amplified into something much more significant because it is able to trigger a release of potential energy from the density field.

In summary, the overall amount of work done by surface buoyancy forces seems to be the same whether or not a conveyor circulation is active. This is possible because the conveyor's northward heat transport is balanced energetically between a positive (cooling) effect in the Northern Hemisphere and a negative (warming) effect in the Southern Hemisphere. Most of the heating and cooling associated with the conveyor seems to be a passive response to a circulation that moves Southern Hemisphere heat to the Northern Hemisphere. The energy dissipated by the conveyor is drawn from the APE

in the ocean's large-scale density field. As shown in the previous section, all the energy drawn from the large-scale density field could come from the winds driving the ACC.

## 6. Concluding remarks

A conventional thermohaline circulation operating with vertical mixing rates $>0.3$ cm$^2$ s$^{-1}$ demands a large energy input from surface buoyancy forces to generate density differences in the ocean's interior. Most of the work in this case is expended to force deep water to upwell in low latitudes. Results in this paper show that the winds that drive the ACC can produce similar density differences and similar levels of overturning with no vertical mixing and no deep upwelling in low latitudes. We show specifically that an Atlantic conveyor closed by upwelling south of the ACC can function with very little energy input from surface buoyancy forces.

All the water in the ocean's interior north of the ACC is warmer and less dense because of the large standing stock of APE maintained in the ocean's interior by the ACC. This means that the density contrast between the new deep water sinking in the North Atlantic and ambient Atlantic water can be enhanced by the effect of winds in the south. Stronger winds applied to the ACC push Atlantic isotherms even deeper—as in the 1.5× experiment of Toggweiler and Samuels (1995). This further enhances the density contrast between sinking water and ambient water. An enhanced density contrast increases the APE drawdown when new deep water forms, making more energy available to the overturning.

Higher salinities and colder temperatures in the far North Atlantic can also enhance the density contrast and the APE drawdown associated with deep-water formation (e.g., Rahmstorf and England 1997). But higher salinities and colder temperatures seem to put very little mechanical energy into the system. The work done by surface buoyancy forces in the North Atlantic seems to act mainly as a trigger that releases potential energy put into the system by the winds driving the ACC.

*Acknowledgments.* We would like to dedicate this paper to Bram Oort on the occasion of his retirement from GFDL in October 1996. Oort's many contributions to the study of the energy cycles in the ocean and atmosphere clearly paved the way for this venture. We would like to acknowledge very helpful reviews by Eli Tziperman, Mike Winton, Jorge Sarmiento, Ellen Druffel, Jerry Mahlman, and two unknown reviewers. Wendy Marshall helped prepare the text and tables. Jeff Varanyak and Cathy Raphael helped prepare the figures.

REFERENCES

Broecker, W. S., 1991: The Great Ocean Conveyor. *Oceanography,* **4,** 79–89.

Bryan, F., 1986: High latitude salinity effects and interhemispheric thermohaline circulations. *Nature,* **323,** 301–304.

——, 1987: Parameter sensitivity of primitive equation ocean general circulation models. *J. Phys. Oceanogr.,* **17,** 970–985.

Bryan, K., 1969: A numerical method for the study of the circulation of the world ocean. *J. Comput. Phys.,* **4,** 347–376.

——, and L. J. Lewis, 1979: A water mass model of the World Ocean. *J. Geophys. Res.,* **84,** 2503–2517.

Cai, W., and P. G. Baines, 1996: Interactions between the thermohaline- and wind-driven circulations and their relevance to the dynamics of the Antarctic Circumpolar Current in a coarse-resolution global ocean general circulation model. *J. Geophys. Res.,* **101,** 14 073–14 093.

Cox, M. D., 1989: An idealized model of the world ocean. Part 1: The global scale water masses. *J. Phys. Oceanogr.,* **19,** 1730–1752.

Cummins, P. F., G. Holloway, and A. E. Gargett, 1990: Sensitivity of the GFDL ocean general circulation model to a parameterization of vertical mixing. *J. Phys. Oceanogr.,* **20,** 817–830.

Gill, A. E., 1982: *Atmosphere–Ocean Dynamics.* Academic Press, 662 pp.

Hellerman, S., and M. Rosenstein, 1983: Normal monthly wind stress over the world ocean with error estimates. *J. Phys. Oceanogr.,* **13,** 1093–1104.

Holland, W. R., 1975: Energetics of baroclinic oceans. *Proc. Symp. on Numerical Models of Ocean Circulation,* Washington, D.C., Natl. Acad. Sci., 168–177.

Ivchenko, V. O., A. M. Treguier, and S. E. Best, 1997: A kinetic energy budget and internal instabilities in the Fine Resolution Antarctic Model. *J. Phys. Oceanogr.,* **27,** 5–22.

Ledwell, J. R., A. J. Watson, and C. S. Law, 1993: Evidence for slow mixing across the pycnocline from an open-ocean tracer-release experiment. *Nature,* **364,** 701–703.

Levitus, S., 1982: *Climatological Atlas of the World Ocean.* NOAA Prof. Paper No. 13, U.S. Govt. Printing Office, Washington, D.C., 163 pp.

Lorenz, E. N., 1955: Available potential energy and the maintenance of the general circulation. *Tellus,* **7,** 157–167.

Munk, W. H., 1966: Abyssal recipes. *Deep-Sea Res.,* **13,** 707–730.

Oort, A. H., S. C. Ascher, S. Levitus, and J. P. Peixoto, 1989: New estimates of the available potential energy in the world ocean. *J. Geophys. Res.,* **94,** 3187–3200.

——, L. A. Anderson, and J. P. Peixoto, 1994: Estimates of the energy cycle in the oceans. *J. Geophys. Res.,* **99,** 7665–7688.

Pacanowski, R. C., K. Dixon, and A. Rosati, 1991: The GFDL Modular Ocean Model users guide. Version 1.0, GFDL Ocean Group Tech. Rep. No. 2, 13 pp. [Available from Geophysical Fluid Dynamics Laboratory/NOAA, Princeton, NJ 08542.]

Polzin, K. L., J. M. Toole, J. R. Ledwell, and R. W. Schmitt, 1997: Spatial variability of turbulent mixing in the abyssal ocean. *Science,* **276,** 93–96.

Rahmstorf, S., 1996: Comment on ''Instability of the thermohaline circulation with respect to mixed boundary conditions: Is it really a problem for realistic models?'' *J. Phys. Oceanogr.,* **26,** 1099–1105.

——, and M. H. England, 1997: The influence of Southern Hemisphere winds on North Atlantic deep water flow. *J. Phys. Oceanogr.,* **27,** 2040–2054.

Rooth, C., 1982: Hydrology and the ocean circulation. *Progress in Oceanography,* Vol. 11, Pergamon, 131–149.

Stuiver, M., P. D. Quay, and H. G. Ostlund, 1983: Abyssal water carbon-14 distribution and the age of the world oceans. *Science,* **219,** 849–851.

Toggweiler, J. R., and B. Samuels, 1993: New radiocarbon constraints on the upwelling of abyssal water to the ocean's surface. *The Global Carbon Cycle,* M. Heimann, Ed., NATO ASI Series, Vol. I 15, Springer-Verlag, 334–366.

——, and ——, 1995: Effect of Drake Passage on the global thermohaline circulation. *Deep-Sea Res.,* **42,** 477–500.

——, K. Dixon, and K. Bryan, 1989: Simulation of radiocarbon in a coarse-resolution world ocean model. 1, Steady state prebomb distributions. *J. Geophys. Res.,* **94,** 8217–8242.

——, E. Tziperman, Y. Feliks, K. Bryan, S. M. Griffies, and B. Samuels, 1996: Reply (to comment by S. Rahmstorf). *J. Phys. Oceanogr.,* **26,** 1106–1112.

Toole, J. M., K. L. Polzin, and R. W. Schmitt, 1994: Estimates of diapycnal mixing in the abyssal ocean. *Science,* **264,** 1120–1123.

Warren, B. A., 1981: Deep circulation of the world ocean. *Evolution of Physical Oceanography, Scientific Surveys in Honor of Henry Stommel,* B. A. Warren and C. Wunsch, Eds., The MIT Press, 6–41.

Whitworth, T., and R. G. Peterson, 1985: Volume transport of the Antarctic Circumpolar Current from bottom pressure measurements. *J. Phys. Oceanogr.,* **15,** 810–816.

Winton, M., 1997: The damping effect of bottom topography on internal decadal-scale oscillations of the thermohaline circulation. *J. Phys. Oceanogr.,* **27,** 203–208.